Critical contribution of 3' non-seed base pairing to the *in vivo* function of the evolutionarily conserved *let-7a* microRNA

Ye Duan[1], Isana Veksler-Lublinsky[2], Victor Ambros[1,*]

[1] Program in Molecular Medicine, University of Massachusetts Medical School, Worcester, MA, 01605, USA

[2] Department of Software and Information Systems Engineering, Ben-Gurion University of the Negev, Beer-Sheva, 8410501, Israel

[*] Corresponding author: victor.ambros@umassmed.edu

Running Title: 3' non-seed region is critical for *let-7a in vivo* function

Key Words: microRNA, *let-7*, *lin-41, let-7 family,* microRNA seed, microRNA non-seed, CRISPR, post-transcriptional regulation, *daf-12*, *hbl-1*

Abstract:

MicroRNAs are endogenous regulatory non-coding RNAs that exist in all multi-cellular organisms. Base-pairing of the seed region (g2-g8) is essential for microRNA targeting, however, the *in vivo* functions of the 3' non-seed region (g9-g22) are less well understood. Here we report the first systematic investigation of the *in vivo* roles of 3' non-seed nucleotides in microRNA *let-7a,* whose entire g9-g22 region is conserved among bilaterians. We found that the 3' non-seed sequence functionally distinguishes *let-7a* from its family paralogs. The complete pairing of g11-g16 is essential for *let-7a* to fully repress multiple key targets, including evolutionarily conserved *lin-41*, *daf-12* and *hbl-1*. Nucleotides at g17-g22 are less critical but may compensate for mismatches in the g11-g16 region. Interestingly, the 3' non-seed pairing of *let-7a* can be critically required even with sites that permit perfect seed pairing. These results provide evidence that the specific configurations of both seed and 3' non-seed base-pairing can critically influence microRNA function *in vivo.*

Introduction

MicroRNAs (miRNA) are short non-coding RNAs that exist in all metazoans (Friedman et al., 2009; Lee et al., 1993; Nelson and Ambros, 2021). Mature miRNAs are bound by Argonaute proteins (AGO) to form the miRNA-induced silencing complex (miRISC), and base pair with complementary sites in the 3' untranslated region (UTR) of target RNAs. miRISC binding leads to post-transcriptional repression of target gene expression through translational inhibition and/or target RNA destabilization (Bartel, 2018). miRNAs are critical for the regulation of diverse physiological processes across species (Ambros, 2004; Bartel, 2018). Up to 60% of human genes are estimated to be regulated by miRNAs, and disfunction of miRNAs is implicated in multiple human diseases (Friedman et al., 2009; Paul et al., 2018).

The miRNA seed corresponds to the 6-7 contiguous nucleotides beginning at the second nucleotide (g2) from 5' end and is understood to be the dominant determinant of miRNA targeting efficacy and specificity. Structural and biochemical studies indicate that miRNA seed, especially g2-g5, is critical for target recognition and binding (Salomon et al., 2015; Schirle et al., 2014). Complementarity to the miRNA seed is the most evolutionarily conserved feature of miRNA target sites, and genetically disrupting seed complementarity can result in de-repression of miRNA targets (Lai, 2002; Lewis et al., 2005; Lim et al., 2005).

Organisms commonly contain multiple genes encoding miRNAs with identical seed sequences, which are grouped into seed families. miRNAs of the same family can in principle recognize shared targets through seed pairing and thereby function redundantly (Abbott et al., 2005; Alvarez-Saavedra and Horvitz, 2010; Brenner et al., 2012). Meanwhile, miRNAs with identical seed but divergent 3' non-seed nucleotides (g9-g22) can exhibit target site selectivity driven by the extent of non-seed base pairing (Broughton et al., 2016; Wahlquist et al., 2014).

The *let-7 (lethal-7) family* miRNAs are distributed widely across the bilaterians, consistent with evolutionary origins in a bilaterian ancestor (Hertel et al., 2012; Wolter et al., 2017). Similarities in the developmental profile of *let-7 family* miRNAs across diverse species and genetic analysis in model organisms suggest evolutionary conservation of *let-7a family* functionality (Roush and Slack, 2008; Tennessen and Thummel, 2008). In nematodes, *let-7 family* miRNAs function in the heterochronic gene pathway to promote the stage-specific cell fate transitions during larval development (Abbott et al., 2005; Reinhart et al., 2000). Similarly, *let-7 family* miRNAs control cellular transitions from pluripotency to differentiation and function in tumor suppression in mammals, and the timing of adult fates during metamorphosis in insects (Balzeau et al., 2017; Lee et al., 2016; Sokol et al., 2008).

Notably, almost all bilaterian genomes encode at least one *let-7 family* isoform (*let-7a*), in which all nucleotides in the 3' non-seed region are highly conserved (Fig. S1A) (Hertel et al., 2012; Pasquinelli et al., 2003). This deep conservation suggests that the 3' non-seed region may also be associated with essential functions which evolutionarily constrained the sequence. Indeed, high-throughput analyses suggested that miRNA 3' non-seed regions can contribute substantially to miRNA-target interactions (Grosswendt et al., 2014; Helwak et al., 2013). Pairing to the 3' non-seed region, especially g13-g16, is thought to enhance target repression in certain contexts (Brennecke et al., 2005; Grimson et al., 2007). Recent structural studies of human AGO complexed with miRNA and target also revealed that g13-g16 can form an A-form helix with the target within miRISC, and can thereby increase miRISC-target affinity and specificity (Sheu-Gruttadauria et al., 2019b; Xiao and MacRae, 2020). Notably, some miRNA target sites have imperfect complementarity with the miRNA seed, such as GU base pair or nucleotide bulge, and are accompanied by extensive non-seed pairing (Chi et al., 2012; Grimson et al., 2007; Vella et al., 2004). In such cases, the 3' non-seed pairing is thought to compensate for the imperfect seed pairing and this compensatory configuration can determine the target specificity among family

isoforms (Brancati and Grosshans, 2018; Brennecke et al., 2005; Doench and Sharp, 2004). However, the relative contributions of specific 3' non-seed nucleotides to the *in vivo* function of miRNAs remain unclear.

Here, we report a systematic investigation of how the 3' non-seed nucleotides contribute to the *in vivo* function of the evolutionarily conserved *let-7a*. We employ CRISPR/Cas9 genome editing of *C. elegans* to systematically introduce defined mutations into the *let-7a* and its conserved target *lin-41*. We show that the sequence of g11-g16 is essential for *let-7a in vivo* function, whilst g17-g22 pairing is less critical than g11-g16 pairing, but can partially compensate for mismatches in g11-g16. We confirm that the 3' non-seed sequence of *let-7a* confers specificity relative to its family paralogs. Furthermore, we show that *lin-41*, as well as heterochronic genes *daf-12* and *hbl-1,* are *let-7a* targets that require 3' non-seed pairing, and that proper repression of *lin-41* requires complementarity to both the seed and critical 3' non-seed region of *let-7a*. Strikingly, the 3' non-seed pairing is functionally required even when the *lin-41* 3' UTR was mutated to accommodate perfect seed pairing, suggesting that the g11-g16 of *let-7a* engage in essential interactions that, in parallel with seed pairing, influence miRISC repressing activity.

Results

The 3' non-seed sequence is essential for the *in vivo* functional specificity of *let-7a* compared to paralogs.

An examination of the phylogenetic distribution of *let-7 family* miRNA genes (Fig. 1A, S1B) emphasizes the presence of *let-7 family* in most bilaterians with available miRNA annotations in miRbase 22.1 (Kozomara et al., 2019). 91.5% (n=117) of bilaterian species have at least one *let-7 family* isoform with no more than 3 different nucleotides from *let-7a* (Fig. S1C-E). Alignment of the isoforms closest to *let-7a* from each of the 117 bilaterian species indicates that all the g9-g22 nucleotides exhibit conservation ranging from 86% to 99%, and 75.2% of the 117 species contain

a *let-7* miRNA completely identical to *let-7a* (Fig. 1B, S1F). This degree of conservation is not observed for other conserved miRNAs (Fig. S1G-H). The deep conservation of *let-7a* suggests that *let-7a* is associated with essential functions that depend on the identity of the 3' non-seed nucleotides.

To test the hypothesis that the 3' non-seed nucleotides are critical for *let-7a in vivo* function, we used CRISPR/Cas9 to mutate the endogenous *let-7a* in *C. elegans* by swapping its 3' non-seed sequence with the sequence of its closest paralog *miR-84* (Fig. 2A). In the resulting *let-7(ma341*) mutant, the passenger strand was also mutated to preserve the precursor miRNA (pre-miRNA) structure. The temporal expression profile of *miR-84* miRNA in *let-7(ma341)* is consistent with expression from the endogenous *mir-84* locus (starting in L2) combined with expression from the edited *let-7* locus (peaking in L4) (Fig. 2B-C). Moreover, in the *mir-84(n4037,null)* background, *miR-84* expression from the *let-7(ma341)* locus alone exhibits a temporal profile similar to that of normal *let-7a* (Fig. 2D-E). Note that the detection method stringently distinguishes *let-7a* from *miR-84*, as *let-7a* was not detected in *let-7(ma341)* animals and *miR-84* was not detected in *mir-84(n4037)* animals (Fig. 2C-E). These results confirm that *let-7(ma341)* expresses *miR-84* miRNA instead of *let-7a*.

In wild-type (WT) animals, the seam cells (hypodermal stem cells) go through asymmetric divisions at each larval stage as one daughter cell differentiates to Hyp7 cells (hypodermis) while the other remains stem cell (Sulston et al., 1983). At L4 molt, the seam cells exit the cell cycle, fuse, and produce the adult-specific cuticle structure referred to as adult alae. In *let-7(ma341)*, we found that seam cells underwent an extra round of cell division after L4 molt, resulting in extra seam cells and incomplete alae in young adults (Fig. 2F-G, Table S1), and *let-7(ma341)* adults exhibited impaired expression of the adult-specific hypodermal reporter COL-19::GFP (Fig. 2H-I). These results indicate that *let-7(ma341)* causes retarded heterochronic phenotypes. *let-7(ma341)* also exhibits lethality as a consequence of bursting at the vulva (Fig. 2J-L). The lethality and

retarded phenotypes are consistent with *let-7a loss-of-function (lf)* phenotypes (Reinhart et al., 2000), indicating that the *in vivo* function of *let-7a* cannot be substituted by its closest paralog *miR-84,* even when *miR-84* is expressed in a developmental profile essentially identical to *let-7a*. Since *let-7a* and *mir-84* share the seed sequence, these findings indicate that the 3' non-seed sequence is a critical determinant of the *in vivo* function and specificity of *let-7a*.

Nucleotides 11-16 are each functionally essential for *let-7a in vivo.*

We next sought to characterize how each 3' non-seed nucleotide contributes to *in vivo* function of *let-7a*. We performed a single nucleotide mutational screen of the *let-7a* non-seed region using the "jump-board" strategy (Duan et al., 2020a). For each g9-g22 nucleotide, we mutated both the miRNA guide and the passenger strands to preserve the pre-miRNA structure (Fig. 3A, S2A). To confirm the expression of the mutant miRNAs, we performed small RNA sequencing of all the mutants and found that the abundance of the mutated *let-7a* miRNA in each mutant was similar to that of the native *let-7a* in WT, with a variance (<10%) that we judge not sufficient to cause *lf* phenotypes by reduced expression (Fig. 3B). Note that the strains with mutations at g11-g16 also contained a WT *let-7* allele on a genetic balancer *umnIs25(mnDp1)*, hence both WT and mutant *let-7a* were expressed.

Single nucleotide mutations at g11, g12, or g13 resulted in severe vulva integrity defects characteristic of *let-7(lf)*, leading to lethality and dramatically reduced numbers of progeny, quantitatively similar to *let-7(null*) (Fig. 3C-D). Single nucleotide mutations at g11-g13 also resulted in impaired expression of COL-19::GFP in Hyp7 cells, and adult alae morphogenesis defects, indicative of retarded heterochronic phenotypes characteristic of severe *let-7(lf)* (Fig. 3C, S2B, Table S1). Single nucleotide mutations at g14-g16 also resulted in phenotypes distinctly characteristic of *let-7(lf)*, although milder than g11-g13 mutations (Fig. 3C-E). By contrast, single nucleotide mutations at g9-g10 or g17-g22 did not cause visible phenotypes (Fig. 3C, F, Table

S1). The mutational screen reveals g11-g16 as a critical non-seed region of *let-7a*, with g11-g13 somewhat more critical than g14-g16 (Fig. 3G).

Nucleotides beyond g16 can compensate for mismatches in the critical non-seed region.

We found that mutating the g18 of *let-7a* into any other three nucleotides did not result in *lf* phenotypes (Fig. S2C). Moreover, simultaneous mutations of g17-g19, g20-g22, or g17-g22 did not cause apparent *lf* phenotypes, even with sensitized conditions like non-physiological temperatures or pathogen-containing cultures (Fig. S2C and data not shown). The insignificance of g17-g22 nucleotides in the screen stands out in contrast with the deep conservation of the entire *let-7a* sequence, especially with g18 as the second most conserved nucleotide (98.3%). We thus hypothesized that g17-g22 may contribute to target repression in cases where mismatches occur within the g11-g16 region.

To test this possibility, we used the *let-7(ma449,* U16G*)* mutation as a genetically sensitized background with moderate phenotypes, and generated a compound mutant *let-7(ma449ma435)* with both U16G and U18A mutations. We observed that *let-7(ma449ma435)* exhibited a strong vulva bursting phenotype and retarded adult alae (Fig. 3H, S2C-D), which are significantly more penetrant than that of each single mutant. We suggest that g18, and by implication other g17-g22 nucleotides, may contribute to interactions that involve mismatches in the g14-g16 sub-critical region.

It is also possible that g17-g22 pairing could be critical for target repression associated with phenotypes that we have not measured here. To investigate this possibility, we assessed molecular phenotypes of *let-7(ma435)* by ribosome profiling and RNA-seq (Fig. S3, Table S2). We found that the expression levels of multiple genes are significantly changed by the U18A mutation, both translationally and transcriptionally, supporting the hypothesis that there are *in vivo* circumstances where *let-7a* g17-g22 nucleotides are critical for proper target regulation.

De-repression of *lin-41* is a major contributor to *let-7a* critical non-seed mutant phenotypes.

Evolutionarily conserved NHL gene *lin-41/Trim71* is a direct target of *let-7a* across species, and repression of *lin-41/Trim71* by *let-7a* is essential for normal development in both invertebrates and vertebrates (Ecsedi and Grosshans, 2013; Worringer et al., 2014). In *C. elegans,* robust repression of *lin-41* by *let-7a* is critical for the L4-to-adult progression, and mutations disrupting the seed pairing between *let-7a* and its complementary sites (LCSs) in the *lin-41* 3' UTR result in reiteration of L4 cell fates and severe vulva defects (Aeschimann et al., 2019). Notably, neither of the two *lin-41* LCSs have perfect seed complementarity with *let-7a* due to a GU pair and a target A-bulge, respectively, while both LCSs contain complementarity to *let-7a* g11-g19, suggesting that 3' pairing may be essential to compensate for the weak seed pairing in this context (Fig. 4A).

We sought to verify whether *lin-41* is de-repressed in the *let*-7a critical non-seed mutants and whether the de-repression causes the *lf* phenotypes. We used the U13A mutant to represent the critical non-seed nucleotides due to its severe phenotypes and the high conservation at g13. At late L4 stage of WT, endogenously tagged GFP::LIN-41 is undetectable in hypodermal cells due to *let-7a* repression (Fig. S4A) (Spike et al., 2014). In contrast, in *let-7(ma432,* U13A*),* we observed elevated peri-nucleolus expression of GFP::LIN-41 in seam and Hyp7 cells, suggesting de-repression of *lin-41* (Fig. S4B). To confirm that the *lin-41* de-repression in *let-7(ma432)* results specifically from disruption of g13 pairing, we restored the native pairing configurations between *let-7(ma432)* and *lin-41* by introducing compensatory mutations at both LCSs in *lin-41* 3' UTR (*ma480*) (Fig. 4A). We did not detect the abnormal expression of GFP::LIN-41 in *lin-41(ma480);let-7(ma432)*, indicating the restoration of *lin-41* repression by re-establishing the WT 3' non-seed pairing configuration (Fig. S4C). We found that in *lin-41(ma480);let-7(ma432),* the *lf* phenotypes caused by *ma432* mutation were substantially rescued based on reduced lethality, increased number of progeny and normal adult alae (Fig. 4B-D, F, Table S1). The rescue of *let-*

7(ma432) phenotypes by restoring g13 pairing indicates that de-repression of *lin-41* is the major contributor to the *lf* phenotypes of *let-7a* critical non-seed mutants.

In parallel, we found that when present with WT *let-7a*, *lin-41(ma480)* exhibited elevated peri-nucleus expression of GFP::LIN-41 in L4 stage, suggesting that disrupting the critical non-seed pairing by mutations in the target sites also causes *lin-41* de-repression (Fig. S3D). As expected, we also observed vulva integrity defects and retarded heterochronic phenotypes in *lin-41(ma480)* (Fig. 4E-F, Table S1), supporting the conclusion that 3' non-seed pairing between *let-7a* and *lin-41* is essential for maintaining the robust repression of *lin-41*.

Disruption of 3' non-seed pairing of *let-7a* results in de-repression of additional targets including *daf-12* and *hbl-1*.

Although *lin-41(ma480);let-7(ma432)* showed alleviation of the *lf* phenotypes from *let-7(ma432),* the double mutant is nevertheless not completely WT and exhibits residual defects in vulva morphogenesis and egg-laying capacity (Fig. 4D, F). Also, COL-19::GFP expression in Hyp7 cells of *lin-41(ma480);let-7(ma432)* adults is reduced at 25 °C, indicating residual retarded phenotypes (Fig. 4G). These residual phenotypes suggest that although *lin-41(ma480);let-7(ma432)* restores the *lin-41* repression, additional *let-7a* targets may be de-repressed by the non-seed mutation (Fig. 4H). We refer to this proposed class of *let-7a* targets that require critical non-seed pairing as "3'-sup targets". Consistent with the reasoning that the phenotypes of *let-7(ma432)* result from the over-expression of both *lin-41* and other 3'-sup targets, the *lin-41(ma480)* mutant, where only *lin-41* is over-expressed since the mutation is on the target, exhibits weaker phenotypes than *let-7(ma432)* (Fig. 4F, Table S1).

To identify the additional *let-7a* 3'-sup targets, we screened for genes that are de-repressed by the *let-7a* critical non-seed mutation. Accordingly, we compared gene expression between WT and *lin-41(ma480);let-7(ma432)* using ribosomal profiling (Ribo-seq), which assesses gene

expression on translational level (Ingolia, 2016). We used *lin-41(ma480);let-7(ma432)* to exclude changes in *lin-41* downstream genes. We found that at L4 stage, 135 genes were significantly over-expressed >2 fold and 351 genes were significantly over-expressed >1.5 fold in *lin-41(ma480);let-7(ma432)* compared to WT (Fig. 5A, Table S3). The translational levels of *lin-41* and its direct downstream genes were not significantly changed, indicating that the de-repressed genes in *lin-41(ma480);let-7(ma432)* are independent of *lin-41* pathway (Fig. S6A) (Aeschimann et al., 2019).

We next sought to identify the *let-7a* 3'-sup targets among the over-expressed genes by identifying LCSs in the 3' UTRs. We developed a computational approach to predict *let-7a* sites involving both seed and critical non-seed complementarity based on the method described in (Veksler-Lublinsky et al., 2010). We firstly identified candidate sites based on seed complementarity to *let-7a,* allowing for both perfect and imperfect pairing at g2-g7, and then extended these sites to check whether they also included at least 3 consecutive base pairs in g11-g16, among which g13 must be paired. We identified 624 genes whose 3' UTR contain *let-7a* 3'-sup sites in *C. elegans,* among which 8 genes are over-expressed in the g13 mutant (Fig. 5A, Table S4). We reasoned that these 8 genes could include *let-7a* 3'-sup targets whose de-repression contributes to the residual phenotypes *lin-41(ma480);let-7(ma432)*.

The heterochronic genes *daf-12* and *hbl-1* were among the 8 candidate 3'-sup targets; and the 3' UTRs of both genes contain multiple *let-7a* sites with critical non-seed pairing (Fig. 5A, S6B-D). We thus suggest that the WT L4-to-adult cell fate transitions require 3' non-seed pairing of *let-7a* to repress not only *lin-41*, but also *daf-12* and *hbl-1*, and accordingly the *daf-12* and *hbl-1* de-repression contributes to the residual retarded phenotypes of *lin-41(ma480);let-7(ma432).* Constant with this supposition, we found that knocking down either *daf-12* or *hbl-1* by RNAi could rescue the abnormal COL-19::GFP pattern in *lin-41(ma480);let-7(ma432)* (Fig. 5B). Interestingly, whereas restoring *lin-41* repression alone could rescue the abnormal adult alae phenotype of *let-*

7(ma432) (Table S1), rescuing the reduced COL-19::GFP in Hyp7 requires restoring repression *daf-12* or *hbl-1* in addition to *lin-41* (Fig. 5B). This suggests that the L4 repression of *lin-41* by *let-7a* is sufficient to regulate adult alae formation, while the robust adult-specific differentiation of Hyp7 requires the repression of *hbl-1, daf-12* and *lin-41*.

Repression of *let-7a* 3'-sup targets can involve translational suppression and/or mRNA decay.

miRNA-mediated post-transcriptional regulation includes translational repression and/or mRNA destabilization, indicated by decreased translational efficiency (TE) and reduced mRNA abundance (Bazzini et al., 2012; Giraldez et al., 2006). It has been shown that *let-7a* can regulate *lin-41* through a combination of both modes (Bagga et al., 2005; Nottrott et al., 2006). To assess the target repression mechanisms associated with *let-7a* 3' non-seed region, we analyzed our Ribo-seq data of *lin-41(m480);let-7(ma432)* in combination with RNA-seq (Fig. 5C, S7, Table S3). Previous reports showed that miRNAs may cause deadenylation before mRNA decay, thus RNAseq libraries from poly(A)-enriched mRNA may potentially have a bias against deadenylated but temporally stable mRNA (Djuranovic et al., 2012; Wu et al., 2006). We thus used ribosomal RNA depletion with anti-sense oligos specifically designed for *C.elegans* to enrich the mRNA (Duan et al., 2020b). We found that the set of de-repressed *let-7a* 3'-sup targets in *lin-41(ma480);let-7(ma432)* include examples of significantly increased mRNA abundance (i.e., *grd-10*) or TE (i.e., *seld-1*, *hbl-1*), or both modes (i.e., *daf-12*), (Fig. 5C). Thus, target recognition involving the *let-7a* non-seed region can elicit inhibition of either TE or mRNA stability, or both, likely depending on context.

Both the seed and non-seed complementarity to *let-7a* are critical for full repression of *lin-41.*

The involvement of 3' non-seed pairing to compensate for imperfect seed pairing has been observed for certain miRNA-target interactions in various systems (Bartel, 2018). However, it remains unclear whether miRISC may elicit other seed-independent functions that critically require non-seed pairing. We anticipated that if 3' non-seed pairing were only required in the context of weak seed pairing, configuring miRNA sites for full seed complementarity should render 3' non-seed pairing unnecessary for target regulation. Therefore, we systematically introduced mutations in the *lin-41* 3' UTR designed to produce various configurations of seed and non-seed pairing with *let-7a* (Fig. 6). Importantly, all the configurations were constructed by mutating both LCSs in *lin-41* and were tested in WT *let-7a* background, so the phenotypes observed should result from de-repression of *lin-41* without confounding effects from other *let-7a* targets.

As noted above, *lin-41(ma480)*, which carries g13:t13 mismatch to WT *let-7a*, exhibited strong retarded heterochronic phenotypes and vulva integrity defects due to *lin-41* de-repression (Fig. 6E). To test whether the g13:t13 mismatch is deleterious only in the context of imperfect seed pairing, we mutated the LCSs of *lin-41(ma480)* to repair the A-bulge and GU pair in the seed pairing. The resulting *lin-41(ma501ma480)* compound mutant is expected to enable consecutive g2-g8 Watson-Crick pairing to *let-7a,* whilst maintaining the g13:t13 mismatch (Fig. 6B). We found that *lin-41(ma501ma480)* animals exhibited a substantial rescue of the *lf* phenotypes from *lin-41(ma480)* (Fig. 6B), confirming the essential compensatory effect of *let-7a* non-seed pairing to imperfect seed complementarity.

Importantly, though *lin-41(ma501ma480)* exhibited full rescue of vulva integrity defects, the rescue of retarded COL-19::GFP expression was incomplete (11% retarded, Fig. 6B), suggesting that enabling perfect seed pairing of *let-7a* was insufficient to fully compensate for the g13:t13 mismatch, and thereby a non-seed mismatch can be deleterious even in the context of perfect

seed pairing. To further explore the requirements for non-seed pairing in the context of perfect seed complementarity, we combined *ma501* with a compound mutation (*ma545*) to mismatch g11-g13 of *let-7a* (Fig. 6C). The LCSs in *lin-41(ma501ma545)* were designed to not permit non-seed pairing with *let-7a* paralogs*.* Interestingly, we found that *lin-41(ma501ma545)* exhibited strong vulva integrity defects and retarded COL-19::GFP expression, suggesting that *lin-41* was de-repressed despite the perfect seed pairing to *let-7a* (Fig. 6C). The loss of *let-7a* regulation in *lin-41(ma501ma545)* indicates that even with perfect seed complementarity, the 3' non-seed pairing still contributes critically to the functional targeting of *lin-41.*

Meanwhile, the full complementarity to *let-7a* seed in *lin-41(ma501)* should in principle enable *let-7a* family paralogs to repress *lin-41*, assuming that perfect seed pairing alone was sufficient to confer full repressing efficacy (Fig. 7A). Since the expression levels of *let-7a* family paralogs *miR-48, miR-84* and *miR-241* combined have been shown to exceed the level of *let-7a* at L4 stage in *C. elegans* (Nelson and Ambros, 2019; Nelson and Ambros, 2021), we anticipated that seed pairing to *lin-41(ma501)* by *let-7a* paralogs might be able to robustly repress *lin-41* in the absence of *let-7a* (Fig. 7C). Strikingly, *lin-41(ma501);let-7a(ma393, null)* only exhibited limited reduction of the severe vulva integrity defects of *let-7a(ma393)*, indicating that the *let-7*a family paralogs only render a minor degree of *lin-41* repression with the engineered "perfect-seed-only" configuration (Fig. 7B). This result further indicates that without 3' critical non-seed pairing, "perfect-seed-only" pairing is insufficient to support fully functional repression of *lin-41*.

We also asked whether 3' non-seed pairing could be sufficient in the absence of seed pairing. We used the previously reported mutation *lin-41(xe11)* which creates an additional seed mismatch to *let-7a* (Fig. 6F) (Ecsedi et al., 2015). We confirmed that *lin-41(xe11)* exhibits strong vulva integrity defects and retarded heterochronic phenotypes (Fig. 6F), indicating that seed pairing of *lin-41 let-7a* is not functionally dispensable, even in the context of extensive 3' pairing.

Discussion

A six-nucleotide critical supplementary pairing region of *let-7a*, involving g11-g16.

It has been shown that the 3' non-seed region of miRNAs can interact with targets and that 3' non-seed pairing has been implicated in compensating for weak seed pairing, for seed family isoform specificity, and target-dependent miRNA degradation (TDMD) (Bartel, 2018; Pawlica et al., 2020). However, no systematic study has been performed to test the contribution of individual 3' non-seed nucleotide to the functional efficacy of miRNA-target interactions in intact animals. The functional architecture of base pairing configurations is particularly interesting for miRNAs with evolutionarily conserved 3' non-seed sequences (i.e., *let-7a*), and for evolutionarily conserved miRNA-target interactions (i.e., *lin-41::let-7a*). In this study, we utilized CRISPR/Cas9 genome editing for a systematic genetic investigation of the *in vivo* function of individual 3' non-seed nucleotide of *let-7a* in the regulation of *lin-41* and other targets in *C. elegans*.

One noteworthy finding from our studies is that single nucleotide mutations at g11-g16 dramatically reduced *let-7a in vivo* function, suggesting their critical contribution to targeting. Previous biochemical analysis and co-crystallized structure of human miRISC-target complex have shown that miRNA can form helix with target at g13-g16, whilst g11 and g12 are structurally hindered from duplexing with target (Grimson et al., 2007; Sheu-Gruttadauria et al., 2019b). In contrast, our results indicate that g11 and g12 of *let-7a* should also duplex with complementary targets. This expanded 3' pairing region (g11-g16) of *let-7a* suggests that miRISC can adopt a previously unanticipated conformation that enables extended 3' pairing from g11 to g16.

Structural analyses of miRISC-target complexes reveal that duplexing of the miRNA seed to target triggers conformational changes of AGO that then enable 3' pairing (Sheu-Gruttadauria et al., 2019b). We note that the structural studies thus far have been for instances of perfect seed pairing. By contrast, for the evolutionarily conserved *let-7a* target *Trim71/lin-41,* the LCSs are

characterized by imperfect seed pairing accompanied by 3' pairing involving g11 and g12 in many species, and in some instances the specific configuration of seed mismatches is conserved, for example the g6:t6-GU pair and t5-bulge across *24 Caenorhabditis* species (Nelson and Ambros, 2021). We suggest that these mismatched seed configurations may promote the AGO conformation that favors the pairing of g11 and g12, in addition to the previously identified 3' pairing region at g13-g16. Meanwhile, it has been shown that the miRISC conformation can also be affected by certain 3' pairing configurations. For example, an alternative AGO conformation can be induced when 3' pairing extends to the 3' end of the miRNA in the context of TDMD (Sheu-Gruttadauria et al., 2019a). We thus suggest that at least for the *let-7a::lin-41* interaction, miRISC may adopt a characteristic novel conformation that reflects simultaneous accommodation of both the imperfect seed pairing and the extended 3' helix.

The necessity of non-seed pairing for target repression efficacy.

It has long been recognized that perfect seed complementarity can be sufficient for miRISC to bind and repress target mRNAs (Brennecke et al., 2005; Doench and Sharp, 2004; Wee et al., 2012), and therefore 3' pairing should be required only to provide compensatory binding in cases of weak seed pairing. However, studies of binding kinetics indicate that 3' pairing can enable miRNA isoforms with identical perfect seed pairing to compete for target recognition (Xiao and MacRae, 2020), highlighting the roles of 3' pairing in addition to the compensatory effect.

In our study, we find that for *lin-41* LCS mutations that enable perfect seed complementarity to *let-7a*, the WT 3' non-seed pairing is still necessary for *let-7a* to confer functional repression of *lin-41* (Fig. 6). Similarly, we show that *let-7a* family paralogs can confer only a modest degree of repression of *lin-41* via engineered perfect seed pairing (Fig. 7). These findings run counter to the assumption that perfect seed pairing should be sufficient for miRISC to confer repression, and provide an example of where 3' non-seed pairing is biologically required for the efficacy of an evolutionarily conserved miRNA-target interaction. Moreover, among the predicted sites with *let-*

7a critical non-seed pairing, all the sites in *daf-12* and 4 out of 7 sites in *hbl-1* have perfect seed pairing (Fig. S6); however, *daf-12* and *hbl-1* are nevertheless de-repressed in the *let-7a* g13 non-seed mutant, supporting the conclusion that non-seed pairing can be critical even for sites with perfect seed complementarity.

Currently, we can only speculate about the mechanistic basis for this requirement for 3' pairing in the context of perfect seed match: perhaps certain structural peculiarities of the 3' UTRs render *let-7a* "seed-only" pairing kinetically unfavorable, or perhaps repression of *lin-41* by *let-7a* requires the recruitment of cofactors that recognize certain miRISC conformational features induced by g11-g16 pairing.

Contribution of the 3' non-seed pairing to the target specificity of *let-7* family paralogs.

Recent reports showed that the *C. elegans let-7a* family paralog *miR-48,* which does not regulate *lin-41* in WT*,* can substitute for *let-7a* in repressing *lin-41* if the *lin-41* LCSs were replaced with a site with a perfect seed match plus extensive 3' pairing to *miR-48* (Broughton et al., 2016). It was proposed that the weak seed pairing of *let-7a* to *lin-41* necessitates the 3' pairing, which differs remarkably between *let-7a* and *miR-48*, and consequently determines the targeting specificity whereby *lin-41* is regulated by *let-7a,* not *miR-48* (Brancati and Grosshans, 2018). Thus, as a general principle, it appears that 3' non-seed pairing combined with imperfect seed pairing is a powerful determinant of specificity for miRNAs of the same seed family. This view is supported by our data, which show that *miR-84,* the closest family paralog of *let-7a* in *C. elegans*, does not functionally substitute for absence of *let-7a*. Our data also provide a particularly powerful reinforcement of the previous model of specificity determination since: (1) in our study, *miR-84* is expressed at levels and with temporal profile identical to WT *let-7a*; (2) unlike *miR-48,* which differs from *let-7a* at every non-seed position, *miR-84* has only 5 nucleotides different from *let-7a*.

We also show that the *in vivo* functional distinction between *let-7a* and *miR-84* primarily reflects the specificity of *let-7a* for targeting *lin-41*, in addition to other targets that require 3' non-seed pairing (Fig. S5). Interestingly, in *C. elegans*, *hbl-1* is synergistically repressed by *let-7a* paralogs at L2-to-L3 transition, and by *let-7a* at L4-to-adult transition (Abrahante et al., 2003; Grosshans et al., 2005; Ilbay and Ambros, 2019). Notably, *hbl-1* 3' UTR contains sites expected to be specifically recognized by *let-7a* (through imperfect seed + 3'-sup), and sites that can be recognized by any paralog in *let-7 family* (through perfect seed) (Fig. S6D). Since we found that functional repression of *hbl-1* in L4 stage requires 3' non-seed pairing (Fig. 5), the "imperfect seed + 3'-sup" sites may enable the *let-7a*-specific repression of *hbl-1* in particular tissues and at late larval stages when *let-7a* is expressed, while the sites with perfect seed pairing would presumably mediate repression of *hbl-1* by *let-7 family* paralogs at earlier larval stages and/or in tissues devoid of *let-7a* expression.

Multiplicity of *C. elegans let-7a* targets with 3' non-seed pairing.

Our computational analysis identified 624 genes in *C. elegans* that contain 3' UTR sequences predicted to bind *let-7a* with 3' non-seed pairing. This finding is consistent with previous high-throughput analyses of miRNA-target chimeric ligation products, which also identified multiple *let-7a* targets with 3' non-seed complementarity (Broughton et al., 2016; Grosswendt et al., 2014). By ribosome profiling, we confirmed that 3' non-seed pairing is critical for the *let-7a* repression of at least 8 genes and that over-expression of *daf-12* and *hbl-1* contribute to the developmental phenotypes of the *let-7a* g13 mutant (Fig. 5). This finding indicates that in addition to *lin-41*, at least *daf-12* and *hbl-1* are also phenocritical *let-7a* targets in *C. elegans* (Ecsedi et al., 2015). We did not test the phenotypic consequences of the other over-expressed *let-7a* 3'-sup targets, which are not known to be involved in the heterochronic pathway. These genes could contribute to *let-7a* phenotypes not assayed in this study.

There are limitations to the use of ribosome profiling of whole animals for the confirmation of *in vivo* miRNA targeting. In particular, the data could contain numerous false negatives, especially for broadly-expressed genes that are repressed by miRNAs in only specific tissues or cell types. For example, in our analysis, although we identified eight target genes with 3' non-seed complementarity that were upregulated in the *let-7a* g13 mutant, as a class, genes with such complementarity were not statistically enriched (Fig. S5E). Similarly, potential *let-7a* target genes with g18 pairing were also not statistically enriched among the de-repressed genes in *let-7* g18 mutant (Fig. S2 and data not shown).

Constraints of the evolutionary conservation of *let-7a* sequence.

The entire *let-7a* sequence is almost perfectly conserved across bilaterian phyla (Fig.1) (Wolter et al., 2017), suggesting phylogenetically ubiquitous involvement of *let-7a* in interactions that constrain the g9-g22 sequence. Our results indicate that the conservation of g11-g16 of *let-7a* could be driven by their phenocritical roles in the repression of conserved targets (i.e., *lin-41*/*Trim71*). Importantly, sequence constraints by target pairing require a multiplicity of targets with a given pairing configuration (John et al., 2004). Our finding of the multiplicity of *let-7a* targets with critical non-seed pairing supports the hypothesis that the 3'-sup pairing could constrain the sequence of g11-g16.

In contrast to the g11-g16 sequence, our data do not appreciably illuminate potential mechanisms for the conservation of *let-7a* 3' distal nucleotides (g17-g22), or the bridge nucleotides (g9-g10). However, although single nucleotide or compound mutations were phenotypically tolerated in g17-g22, we observed phenotypic effects of a g18 mutation in the context of g16 mutation, suggesting involvement of 3' distal nucleotides in repressing targets with obligate mismatches to g14-g16 to *let-7a*. It is also possible that *let-7a* 3' distal nucleotides could interact with miRISC associated sequence-specific RNA binding proteins in certain contexts. Meanwhile, mutations at g9-g10 were also phenotypically tolerated, consistent with the

observation that *let-7a* is not predicted to engage in target recognition involving g9-g10 paring in *C. elegans*, and that fully complementary target sites which involve the bridge pairing are rare in vertebrates (Bartel, 2018). However, miRNA bridge nucleotides can be exposed on the miRISC surface even when they are complementary to the target (Sheu-Gruttadauria et al., 2019a). We thus hypothesize that g9-g10 of *let-7a* may be constrained by association with conserved RNA binding proteins that recognize these nucleotides, perhaps in the context of *let-7a* biogenesis or target binding.

It is also possible that the identity of g9-g10 or g17-g22 nucleotides of *let-7a* could be critical for target repression under unconventional conditions (i.e., stress), and/or required for target interactions unrelated to the phenotypes that we monitored. The latter possibility is supported by our analysis that the g18 mutant displays molecular phenotypes by Ribo-seq and RNA-seq (Fig. S3). Such molecular phenotyping of other distal 3' nucleotides of *let-7a*, and other 'silent' nucleotides of other miRNAs, could reveal otherwise experimentally inaccessible functionalities.

Acknowledgment

This research was supported by funding from NIH grants R01GM088365, R01GM034028 and R35GM131741 (V.A.). Some *C. elegans* strains were provided by the CGC, which is funded by NIH Office of Research Infrastructure Programs (P40 OD010440).

Author Contribution:

Conceptualization: Y.D, I.V-L, V.A; Methodology: Y.D, I.V-L., V.A.; Formal analysis: Y.D, I.V-L., V.A.; Investigation: Y.D, I.V-L.; Resources: I.V-L., V.A.; Data curation: Y.D.; Writing - original draft: Y.D.; Writing - review & editing: Y.D., I.V-L., V.A.; Supervision: V.A.; Project administration: V.A.; Funding acquisition: V.A.

Figure 1. *let-7a* is deeply conserved at all nucleotides across bilaterian species. A. Summary of *let-7 family* miRNAs across bilaterian phylogeny. Bar length, number of *let-7 family* members; bar color, sequence distances to *hsa-let-7a-5p*. **B.** Nucleotide frequency of the *let-7 family* isoforms most similar to *hsa-let-7a-5p* across bilaterians.

Figure 2. The 3' non-seed sequence determines the functional specificity of *let-7a* among its paralogs. A. Strategy of the *miR-84* swap mutagenesis. The dot-bracket notations show the pre-miRNA structures predicted by RNAfold (Denman, 1993). **B-E.** Developmental profiles of *miR-84* and *let-7a* miRNAs determined using Fireplex assays. Expression levels are calibrated with synthetic *miR-84* and *let-7a* oligos. **F.** Representative lineages and COL-19::GFP expression patterns of V1-V4 and V6 seam cells in WT and *let-7(ma341)*. **G.** Seam cell numbers of young adults. **H-I.** Representative expression patterns of COL-19::GFP in adults. Scale bars, 100 µm. **J-K.** DIC images of the vulva region of adults. Scale bars, 25 µm. **L.** Adult lethality for WT, *let-7(ma341)*, *let-7(n2853,* seed mutant), and *let-7(ma393, null)*. Lethal phenotypes are categorized as either with vulva bursting (severe) or egg laying defective (mild).

Figure 3. Contribution of single 3' non-seed nucleotides to the *in vivo* function of *let-7a.* A. Alignment of the mutants' pre-miRNA sequences in the single nucleotide mutational screen. The non-seed region is boxed. **B.** Small RNA sequencing reads (prepared from L4 larvae) that mapped to WT or mutant *let-7a* sequences for each single mutant. The reads mapping to WT *let-7a* for strains carrying the mutations of g11-g16 include WT *let-7a* miRNA from the balancer *mnDp1.* **C.** Phenotype penetrance of COL-19::GFP pattern (top), numbers of progeny (middle) and lethality (bottom). Lethal phenotypes are categorized identically to Fig. 2L. Abnormal COL-19::GFP patterns are categorized as no Hyp7 expression (severe) or faint Hyp7 expression (mild). **D-G.** DIC images of the vulva region in adults of *let-7(ma432)*(**D**); *let-7(ma449)*(**E**); *let-7(m435)*(**F**) and *let-7(ma449ma435)*(**G**) at 25 °C. Scale bars, 25 µm. **H.** Functional synergy between g18 region and the critical non-seed region. Labels are identical to **C** (bottom). **G.** Summary of the

functional merits of *let-7a* 3' non-seed nucleotides. Colored circle, 3' non-seed nucleotide; red proportion, average penetrance of the severe vulva integrity phenotype at all temperatures.

Figure 4. The *let-7a* critical non-seed nucleotides confer *in vivo* function by repressing both *lin-41* and additional 3'-sup targets. A. Pairing configurations between *let-7a* and *lin-41* LCS1/2. **B-E.** DIC images of the adult vulva regions representative of *lin-41(tn1541)*(**B**), *lin-41(tn1541);let-7(ma432)*(**C**), *lin-41(tn1541ma480);let-7(ma432)*(**D**) and *lin-41(tn1541ma480)*(**E**) at 25 °C. Scale bars, 25 µm. **F.** Vulva integrity defects based on lethality (bottom) and the number of progeny (top). Lethal phenotypes are categorized identically to Fig. 2L. **G.** Representative COL-19::GFP pattern and penetrance of *lin-41(tn1541ma480);let-7(ma432)* young adults at 25 °C. Scale bars, 100 µm. **H.** Illustrative models proposing that both *lin-41* and additional 3'-sup targets are de-repressed in *let-7a* non-seed mutants.

Figure 5. *let-7a* represses a multiplicity of 3'-sup targets, including *daf-12* and *hbl-1*, through 3' non-seed pairing. A. Differential expression analysis of translatomes of *lin-41(tn1541ma480);let-7(ma432)* and *lin-41(tn1541)*. Volcano plot represents genes with increased ribosome protected footprints (RPFs) in *lin-41(tn1541ma480);let-7(ma432)* compared to *lin-41(tn1541).* Solid points, significantly increased genes (FC > 1.5, P.adj < 0.1 by DESeq2). Circled points with text labels, genes with predicted *let-7a* 3'-sup sites; triangle points, genes with only *let-7a* seed-only sites. **B.** Retarded COL-19::GFP patterns characteristic of *lin-41(tn1541ma480);let-7(ma432)* young adults at 25 °C under empty vector conditions (top), *daf-12(RNAi)* (middle) or *hbl-1(RNAi)* (bottom). Scale bars, 100 µm. **C.** Fold changes of mRNA abundance and translational efficiency (TE), comparing *lin-41(tn1541ma480);let-7(ma432)* to *lin-41(tn1541)*. Red/orange points, genes with significantly increased mRNA abundance/TE (FC > 1.5, P.adj < 0.1 by DESeq2 for mRNA abundance or P < 0.1 by t-test for TE). Purple points, genes with both significantly increased TE and mRNA abundance. Circled points, genes with

significantly increased RPFs in (**A)**. Predicted *let-7a* 3'-sup targets are text-labeled. Data in **A** and **C** were generated by 3 biological replicas.

Figure 6. Both the critical non-seed and seed paring are functionally critical for *let-7a* in repressing *lin-41.* A-F. Pairing configurations of *let-7a* to the *lin-41* LCSs, and associated phenotypes for *lin-41(tn1541ma501)* (**A**)*; lin-41(tn1541ma501ma480)* (**B**), *lin-41(ma501ma545)* (**C**), *lin-41(tn1541)* (**D**), *lin-41(tn1541ma480)* (**E**), and *lin-41(ex11)* (**F**), arranged in a matrixed panel based on mismatch numbers in seed (vertical axis) and critical non-seed region (horizontal axis). For each panel, phenotypes include major COL-19:GFP pattern and penetrance in adults at 25 °C (middle) and vulva defects (bottom) by adult lethality (bar charts) and numbers of progeny (violin plots). Scale bars, 100 µm. Lethal phenotypes are categorized identically to Fig. 2L.

Figure 7. Perfect seed pairing alone is insufficient for *let-7a* family paralogs to confer full repression of *lin-41*. A. Predicted pairing configurations of *let-7a* and family paralogs *miR-48/84/241* to LCS1 (top) and LCS2 (bottom) of *lin-41(ma501)* transcribed from RNAhybird (Rehmsmeier et al., 2004). **B.** Vulva integrity defects based on adult lethality (top) and number of progeny (bottom) in *lin-41(tn1541), lin-41(tn1541);let-7(ma393,null)* and *lin-41(tn1541ma501);let-7(ma393)*. **C.** Schematic diagrams of predicted targeting configurations.

Methods

Phylogeny and conservation analysis

Precursor and mature miRNA sequences, and a phylogenetic tree of metazoa species were downloaded from miRbase (v22.1) (Kozomara et al., 2019). An in-house code was developed to identify miRNAs that belong to the *let-7 family* based on the presence of the seed sequence "GAGGUA" at g2-g7 on the mature miRNA. For each species in the collection, the number of total miRNA loci and the number *let-7* miRNA loci were counted. To calculate the distance of each member to the conserved *hsa-let-7a*, its sequence was aligned to the *hsa-let-7a* sequence and the number of mismatches in the alignment was counted. The phylogenetic trees were visualized with the program evolView v2 (He et al., 2016).

117 species encode *let-7a* family isoforms. From each species, the sequence of one, the most similar to *let-7a,* was extracted and used to construct a conservation profile. A similar analysis was done with the *mir-1* and *mir-34* families to obtain their conservation profiles.

Targeted mutagenesis at the *let-7a* genomic locus

CRISPR/Cas9 genome editing of *let*-7a locus was performed using the "jump board" strategy described in (Duan et al., 2020a) on strain *VT3742*, which carries the *let-7(ma393)* insertion of the "jump board" sequence in place of the *pre-let-7* sequence, as well as the genetic balancer *mnDp1(umnIs25)*, and a transgene *oxSi1091* expressing Cas9. Templates for dsDNA HR donors were prepared by cloning the wild type pre-*let-7a* and 500 bp of flanking sequence into pCR2.1-TOPO vector. The Q5 mutagenesis kit (NEB, Cat: E0554) was used to generate the mutant plasmids. Double-strand DNA donors were generated from the mutant plasmids by PCR with 73/106 base-pairs flanking the pre-*let-7a,* and the PCR product was purified by ethanol precipitation. Injection mixtures containing final concentrations of 30 ng/µl AltR_Cas-9_crRNA_INPP4A_1/2 each, 10 ng/µl AltR_Cas-9 _crRNA_dpy-10_cn64 as co-CRISPR marker (Arribere et al., 2014), 75 ng/µl Alt-R tracrRNA (IDT, Cat:1072532), 10 ng/µl each dsDNA donor in 1X duplex buffer (IDT, Cat: 11010301) were injected into the gonad of *VT3742* at young adult stage. F1 dumpy animals were isolated and genotyped by PCR with let-7_SEQ_F5/R5 primers followed by an analysis of the PCR product using restriction digestion using EcoRV (NEB, Cat:N3195) and Sanger sequencing as described in (Duan et al., 2020a). Mutants were backcrossed with wild-type (*N2* or *VT1367*) for at least two generations.

Targeted mutagenesis at the *lin-41* genomic locus

Ultramer single-strand DNA donors (lengths ranging from 115 nt to 117 nt) with 35 nt flanking homology were obtained from IDT. The injection mixture containing final concentrations of 25 ng/µl AltR_Cas-9_crRNA_lin-41_1/2 each, 15 ng/µl AltR_Cas-9_crRNA_dpy-10_cn64, 95 ng/µl Alt-R tracrRNA (IDT, Cat:1072532), 325 ng/µl each ssDNA donor in 1X duplex buffer (IDT, Cat: 11010301) were incubated at room temperature for 10 min for pre-annealing and injected into the gonad of *VT3867* or *VT3873* which contain *let-7(ma432)* mutation, *mnDp1(umnIs25)* and transgene *oxSi1091* expressing Cas9. F1 dumpy animals were isolated and genotyped by PCR with lin-41_SEQ_F2/R2 primers, followed by an analysis of the PCR product using Sanger sequencing. Mutants were backcrossed with N2 for at least two generations.

Worm culturing and synchronization

C.elegans were cultured on nematode growth medium (NGM) and fed with *E. coli* HB101 unless specified. To obtain populations of synchronized developing worms, gravid adults were collected and washed twice with water. Pellets of centrifuged worms were treated with 5 ml 1N NaOH and 1% (v/v) sodium hypochlorite for 5 min with shaking to obtain embryos, and the embryos were rinsed with M9 buffer three times. The embryos were hatched in 10 ml M9 buffer at 20°C for 16-18 hrs with mild shaking. Hatched L1 larvae were transferred to plates at 30-50 worms per plate and replicate plates were cultured at 15°C, 20°C, or 25 °C for defined periods; samples of the population were examined by microscopy to confirm the developmental stage at the time of harvest.

Phenotypic assays for vulva defects

The adult lethality characteristic of *let-7(lf)*, which results from rupture of the young adult animal at the vulva, was scored after approximately 36 hrs (15°C), 24 hrs (20°C) or 16 hrs (25°C) of development (when at least 90% of the population had reached the adult stage). To score viable progeny per adult, young adults were transferred to a fresh plate every 12 hrs until those capable of laying eggs had completed egg-laying. Only hatched eggs were counted.

572 **Microscopy and heterochronic phenotypes**

573 Differential interference contrast and fluorescent images were obtained by Zeiss.Z1 equipped
574 with ZEISS Axiocam 503 camera. COL-19::GFP patterns were scored 10X objective. Adult alae
575 and GFP::LIN-41 images were obtained using a 100X objective. Lateral hypodermal
576 heterochronic cell lineage defects were scored by counting the number of seam cells per side of
577 each animal with the aid of the *wIs51* transgenic seam cell reporter. Patterns of expression of the
578 adult-specific COL-19::GFP reporter were scored using the *maIs105* transgenic reporter.
579 Fluorescent images were processed by ImageJ FIJI (Schindelin et al., 2012).

580

581 **RNAi**

582 Overnight cultures of HT115 bacteria expressing dsRNA (Timmons et al., 2001) were
583 transferred to LB broth and shaken at 37 °C until OD_{600} was between 0.4 – 0.8. The bacteria
584 cultures were spread on NGM medium containing 100 µg/ml ampicillin and 1 mM IPTG, and
585 induced at room temperature for 24-48 hrs. HT115 bacteria strains for RNAi were obtained from
586 the Ahringer library (Kamath et al., 2003).

587

588 **Total RNA preparation**

589 Harvested worms were washed with M9 medium, centrifuged, and the worm pellets were flash-
590 frozen in liquid nitrogen. The worm pellets were thawed and lysed by adding 4X volumes of QIAzol
591 (Qiagen, Cat: 79306) and shaking vigorously at room temperature for 15 min. The total RNA was
592 extracted by the addition of 0.85X volume chloroform, centrifugation, and recovery of the aqueous
593 phase, which was then re-extracted with 1 volume phenol:chloroform:isoamyl alcohol (25:24:1,
594 pH = 5.5). Total RNA was then precipitated by add 1 volume of isopropanol and 0.5 µl GlycoBlue
595 (Invitrogen, Cat: AM9516), followed by incubation at -80ºC for at least 30 min, and recovery by
596 centrifugation at 25,000 rcf for 10 min at 4 °C. The supernatants were then removed, and the RNA
597 pellets were subsequently washed twice by 70% (v/v) ethanol, dried in air for 5 min, dissolved in
598 water, and stored at -80ºC.

599

600 **Fireplex miRNA assay**

Synchronized populations of developing worms were cultured at 20 °C and harvested at 8 hrs (L1), 22 hrs (L2), 36 hrs (L3), 46 hrs (L4) and 58 hrs (adult) after feeding. Total RNA was extracted and miRNA levels of *miR-84* and *let-7a* were quantified by FirePlex miRNA assay (Abcam) with customized *C.elegans* miRNA panel following the manufacturer's instructions. Guava easyCyte 8HT (Millipore) was used for readout. To normalize the quantification, synthetic RNA oligonucleotides with sequences of *miR-84* and *let-7a* (IDT) were serially diluted and subjected to FirePlex miRNA assay. Equal amounts of total RNA were used for all the samples and replicates. The amounts of miRNA in experimental samples were calculated from the standard curve generated from the serial dilution of respective synthetic RNA oligonucleotides.

Small RNA sequencing

Synchronized populations of developing worms were cultured at 20 °C and harvested at the mid-late L4 stage (45 hrs after feeding). Total RNA was extracted as described above. The small RNA sequencing libraries were constructed using QIAseq miRNA Library Kit (Qiagen, Cat:331505 & 331595), and sequenced by Illumina NextSeq 500 system. The adaptor sequences were trimmed from the 3' end of the raw reads by *Cutadapt/1.9* using default parameters (Martin, 2011). To quantify the wild type or mutant *let-7a* miRNAs, the trimmed reads were mapped with *Bowtie2/2.3.4.3* to either wild type or mutant *let-7a* sequences indexed with *-c* using parameters *--end-to-end -N 0 --no-1mm-upfront -L 22* (Langmead and Salzberg, 2012). To quantify the total small RNA reads, trimmed reads were size filtered by *Cutadapt/1.9,* and reads with a length between 20-25 bp were kept. The filtered reads were initially mapped with *Bowtie2/2.3.4.3* to *C. elegans* rRNA and tRNA sequences from *WBCel235* with default parameters to remove tRNA and rRNA fragments (Chan and Lowe, 2009, 2016), and remaining reads were mapped to *C. elegans* genome *WBCel235* by *Bowtie2/2.3.4.3* with default parameters. The numbers of reads that mapped uniquely to the genome were used to calculate the RPM of wild type and mutant *let-7a.*

Ribosome Profiling

Worm harvesting

Synchronized populations of developing worms were cultured at 20 °C for 45 hrs after feeding. Harvested worms were washed with water three times and incubated at room temperature for 10

min to allow digestion of intestinal bacteria. Worms were then pelleted by centrifuge at 4,500 rcf for 2 min at room temperature and residual water was removed until the total volumes were twice as the worm pellets. The samples were then flashed frozen by liquid nitrogen and stored at -80 °C.

Monosome preparation

Concentrated lysis buffer was add to each frozen sample to final concentration of 20 mM Tris-HCl (pH = 7.4), 150 mM NaCl, 5 mM $MgCl_2$, 0.5X Protease Inhibitor (Sigma, Cat:P2714), 1 mM DTT, 0.1 mg/ml cycloheximide (Millipore, Cat:C4859), 1% (v/v) Triton X100 and 5 U/ml Turbo DNase (Invitrogen, Cat:AM2238) (Ingolia et al., 2012), and worm pellets were kept on ice until fully thawed. Suspended worms were transferred to 400 µm silica beads tube (OPS Diagnostic, Cat: PFAW-400-100-04) and lysed in bead beater homogenizer for 3 min at 4 °C. Lysates were then centrifuged at 25,000 rcf for 10 min at 4 °C, and supernatants were collected. To generate monosomes, RNase I (Invitrogen, Cat: AM2294) was added to a final concentration of 0.2 U per µl of harvested worm pellet. The digestion was incubated at room temperature for 40 min with gentle rotation and then quenched by adding SUPERase RNase inhibitor (Invitrogen, Cat: AM2694) at 4 U per RNase I unit. The lysates were then loaded onto 5-40 % (m/v) sucrose gradients prepared with lysis buffer without Triton X100 and centrifuged at 32,000 rpm for 3 hrs at 4 °C in an SW41Ti rotor (Beckman Coulter, Cat:331362). The sucrose gradients were fractionated using BR-188 Density Gradient Fractionation System with 60% (m/v) sucrose as chase solution, and monosome fractions were collected according to OD_{254} profiles.

RPF cloning

3.5 X volumes of QIAzol reagent was added to the gradient fractions containing monosomes, and RNA was extracted and separated by 17.5 % denaturing PAGE. A synthetic RNA oligonucleotide with the length of 30 nt was used as a size marker. The gel was stained by Sybr Gold (Invitrogen, Cat: S11494) at room temperature for 10 min, and a gel slice containing RNA of approximately 30 nt was excised and ground by an RNase-free pellet pestle (Fisher Scientific, Cat: 12-141-364). RNA was extracted from the gel slice by adding 500 µl of 300 mM NaAc (pH = 5.5), 1 mM EDTA, and 0.25% (m/v) SDS and mildly shaking overnight at room temperature (Ingolia et al., 2012). The gel granules were excluded using Spin-X tube filter (Millipore, Cat: CLS8160) and the RNA was then concentrated by ethanol precipitation, dissolved in water, and stored at -80 ^{o}C. 5’ phosphorylation and 3’ dephosphorylation were performed with T4 PNK (NEB, Cat: M0201S) following the manufacturer’s instructions, and the products were subjected to phenol/chloroform extraction and ethanol precipitation. cDNA libraries were constructed using

QIAseq miRNA Library Kit (Qiagen, Cat:331505 & 331595) following the manufacturer's instructions, except that the amplifying PCR was conducted with 9-12 cycles, and sequencing was perform using Illumina NextSeq 500 system.

RPF data analysis

The adaptor sequences were trimmed from the 3' end of the raw reads by the *Cutadapt/1.9* software using default parameters (Martin, 2011). Reads were sized filtered to keep only reads with a length between 26-34 bp (a range that fits ribosome-protected fragments) (Aeschimann et al., 2015). The rRNA and tRNA reads were removed by initially mapping with *Bowtie2/2.3.4.3* to *C. elegans* rRNA and tRNA sequences from *WBCel235* with default parameters (Chan and Lowe, 2009, 2016; Langmead and Salzberg, 2012), and the remaining reads were mapped to the *C. elegans* genome *WBcel235* by *Star/2.5.3* with default parameters (Dobin et al., 2013). The p-offset of the 5' end of the mapped reads and the monosome periodicity were determined by *plastid/0.4.8,* and gene counting on exons was generated by *plastid_cs/0.4.8* with p-offset adjusted (Dunn and Weissman, 2016; Santos et al., 2019). Differential expression analysis was performed by *DESeq2* with default parameters (Kucukural et al., 2019; Love et al., 2014). Genes with max raw count smaller than 10 were excluded from the analysis. Volcano plots were generated using *ggplot2* (Hadley, 2016).

mRNA enrichment by *C.elegans* specific ribosome RNA depletion

Worm samples for RNA-seq were aliquoted from the ribosome profiling harvests before the lysis step and frozen separately. The total RNA was extracted as described above. To enrich for mRNA, rRNA was depleted as described in detail elsewhere (Duan et al., 2020b). rRNA-depleted mRNA samples were then purified by RNA Clean & Concentrator-5 Kit (ZYMO, Cat: R1015) (Zhang et al., 2012). The RNA-seq libraries were constructed by NEBNext Ultra II RNA Library Prep kit (NEB, Cat: E7775, E7335, E7500) and sequenced by Illumina NextSeq 500 system (Duan et al., 2020b).

RNA-seq and translational efficiency data analysis

The adaptor sequences were trimmed from RNA-seq data and reads shorter than 15 nt were filtered out from the analysis by *Cutadapt/1.9*. tRNA, signal recognition particle RNA (srpR), and residual cytoplasmic rRNA reads were removed by initial mapping with *Bowtie2/2.3.4.3*, and the

remaining reads were mapped to *C. elegans* genome *WBcel235* by *Star/2.5.3* with default parameters. Gene counting was done by *featureCounts* (Liao et al., 2014). Differential expression analysis was performed by *DESeq2* with default settings (Kucukural et al., 2019; Love et al., 2014). To calculate the translational efficiency (TE), the genes with max raw count smaller than 10 for either RNA-seq or ribosome profiling were excluded from the analysis. The TE was calculated by dividing normalized ribosome profiling counts by normalized RNA-seq counts for each replica. Significance was calculated by the Student t-test. Volcano plots were generated using *ggplot2.*

Target prediction

3' UTR sequences of C.elegans genes were downloaded from WormBase Parasite website (Howe et al., 2016; Howe et al., 2017) for the genomic version *WBcel235*. The UTRs were sorted and filtered to remove redundant sequences. The final dataset contained 15058 3'UTR sequences for 13975 genes (some genes have more than one 3'UTR isoform). The target sites of *let-7a* sequence that obey one of the following criteria were predicted using the algorithm developed in (Veksler-Lublinsky et al., 2010) (1) perfect Watson-Crick complementarity (perfect match) to positions 2-7; (2) perfect match to positions 2-7 allowing 1 target bulge on positions 5-7; (3) perfect match to positions 2-8 allowing 1 GU/Mismatch (MM) on positions 5-8; (4) perfect match to positions 2-7 allowing 1 mRNA bulge on positions 2-4; (5) a match to positions 2-8 allowing 1 GU/MM on positions 2-4.

For sites that obey the criteria, a flanking region of additional 20 nucleotides after the seed was extracted. The interaction duplex between the full site and the miRNA was then calculated using RNAduplex (Lorenz et al., 2011). The duplex was parsed to identify both the seed type and the non-seed type for each reported interaction as follows: (a) Seed type: (1) 2-7 full match ; (2) 2-7 + 1 target bulge on 5-7 or 2-8 with 1GU/MM 5-8; (3) 2-7 + 1 target bulge on 2-4 or 2-8 with 1 GU/MM 2-4. (b) NonSeedType: (1) perfect match to positions 11-13 or 12-14 or 13-16 ; (2) match allowing GUs to positions 11-13 or 12-14 or 13-16; (-1) none of the above.

For genes that have multiple UTR sequences in the analysis, UTRs with redundant duplexes were filtered out from the final report.

Quantification and statistical analysis

All data containing statistical analysis represent the mean ± standard deviation of at least three replications. The p-values representation is as follow: 0.05-0.01(*); 0.01-0.001(**); 0.001-0.0001(***); <0.0001(****). Significance tests were conducted with Prism 8 if not mentioned.

References

Abbott, A.L., Alvarez-Saavedra, E., Miska, E.A., Lau, N.C., Bartel, D.P., Horvitz, H.R., and Ambros, V. (2005). The let-7 MicroRNA family members mir-48, mir-84, and mir-241 function together to regulate developmental timing in Caenorhabditis elegans. Developmental cell *9*, 403-414.

Abrahante, J.E., Daul, A.L., Li, M., Volk, M.L., Tennessen, J.M., Miller, E.A., and Rougvie, A.E. (2003). The Caenorhabditis elegans hunchback-like gene lin-57/hbl-1 controls developmental time and is regulated by microRNAs. Developmental cell *4*, 625-637.

Aeschimann, F., Neagu, A., Rausch, M., and Grosshans, H. (2019). let-7 coordinates the transition to adulthood through a single primary and four secondary targets. Life Sci Alliance *2*.

Aeschimann, F., Xiong, J., Arnold, A., Dieterich, C., and Grosshans, H. (2015). Transcriptome-wide measurement of ribosomal occupancy by ribosome profiling. Methods *85*, 75-89.

Alvarez-Saavedra, E., and Horvitz, H.R. (2010). Many families of C. elegans microRNAs are not essential for development or viability. Current biology : CB *20*, 367-373.

Ambros, V. (2004). The functions of animal microRNAs. Nature *431*, 350-355.

Arribere, J.A., Bell, R.T., Fu, B.X., Artiles, K.L., Hartman, P.S., and Fire, A.Z. (2014). Efficient Marker-Free Recovery of Custom Genetic Modifications with CRISPR/Cas9 in Caenorhabditis elegans. Genetics *198*, 837-846.

Bagga, S., Bracht, J., Hunter, S., Massirer, K., Holtz, J., Eachus, R., and Pasquinelli, A.E. (2005). Regulation by let-7 and lin-4 miRNAs results in target mRNA degradation. Cell *122*, 553-563.

Balzeau, J., Menezes, M.R., Cao, S., and Hagan, J.P. (2017). The LIN28/let-7 Pathway in Cancer. Frontiers in genetics *8*, 31.

Bartel, D.P. (2018). Metazoan MicroRNAs. Cell *173*, 20-51.

Bazzini, A.A., Lee, M.T., and Giraldez, A.J. (2012). Ribosome profiling shows that miR-430 reduces translation before causing mRNA decay in zebrafish. Science *336*, 233-237.

Brancati, G., and Grosshans, H. (2018). An interplay of miRNA abundance and target site architecture determines miRNA activity and specificity. Nucleic acids research *46*, 3259-3269.

Brennecke, J., Stark, A., Russell, R.B., and Cohen, S.M. (2005). Principles of microRNA-target recognition. PLoS biology *3*, e85.

Brenner, J.L., Kemp, B.J., and Abbott, A.L. (2012). The mir-51 family of microRNAs functions in diverse regulatory pathways in Caenorhabditis elegans. PloS one *7*, e37185.

Broughton, J.P., Lovci, M.T., Huang, J.L., Yeo, G.W., and Pasquinelli, A.E. (2016). Pairing beyond the Seed Supports MicroRNA Targeting Specificity. Molecular cell *64*, 320-333.

Chan, P.P., and Lowe, T.M. (2009). GtRNAdb: a database of transfer RNA genes detected in genomic sequence. Nucleic acids research *37*, D93-97.

Chan, P.P., and Lowe, T.M. (2016). GtRNAdb 2.0: an expanded database of transfer RNA genes identified in complete and draft genomes. Nucleic acids research *44*, D184-189.

Chi, S.W., Hannon, G.J., and Darnell, R.B. (2012). An alternative mode of microRNA target recognition. Nature structural & molecular biology *19*, 321-327.

Denman, R.B. (1993). Using RNAFOLD to predict the activity of small catalytic RNAs. BioTechniques *15*, 1090-1095.

Djuranovic, S., Nahvi, A., and Green, R. (2012). miRNA-mediated gene silencing by translational repression followed by mRNA deadenylation and decay. Science *336*, 237-240.

Dobin, A., Davis, C.A., Schlesinger, F., Drenkow, J., Zaleski, C., Jha, S., Batut, P., Chaisson, M., and Gingeras, T.R. (2013). STAR: ultrafast universal RNA-seq aligner. Bioinformatics *29*, 15-21.

Doench, J.G., and Sharp, P.A. (2004). Specificity of microRNA target selection in translational repression. Genes & development *18*, 504-511.

Duan, Y., Choi, S., Nelson, C., and Ambros, V. (2020a). Engineering essential genes with a "jump board" strategy using CRISPR/Cas9. MicroPubl Biol *2020*.

Duan, Y., Sun, Y., and Ambros, V. (2020b). RNA-seq with RNase H-based ribosomal RNA depletion specifically designed for C. elegans. MicroPubl Biol *2020*.

Dunn, J.G., and Weissman, J.S. (2016). Plastid: nucleotide-resolution analysis of next-generation sequencing and genomics data. BMC genomics *17*, 958.

Ecsedi, M., and Grosshans, H. (2013). LIN-41/TRIM71: emancipation of a miRNA target. Genes & development *27*, 581-589.

Ecsedi, M., Rausch, M., and Grosshans, H. (2015). The let-7 microRNA directs vulval development through a single target. Developmental cell *32*, 335-344.

Friedman, R.C., Farh, K.K., Burge, C.B., and Bartel, D.P. (2009). Most mammalian mRNAs are conserved targets of microRNAs. Genome research *19*, 92-105.

Giraldez, A.J., Mishima, Y., Rihel, J., Grocock, R.J., Van Dongen, S., Inoue, K., Enright, A.J., and Schier, A.F. (2006). Zebrafish MiR-430 promotes deadenylation and clearance of maternal mRNAs. Science *312*, 75-79.

Grimson, A., Farh, K.K., Johnston, W.K., Garrett-Engele, P., Lim, L.P., and Bartel, D.P. (2007). MicroRNA targeting specificity in mammals: determinants beyond seed pairing. Molecular cell *27*, 91-105.

Grosshans, H., Johnson, T., Reinert, K.L., Gerstein, M., and Slack, F.J. (2005). The temporal patterning microRNA let-7 regulates several transcription factors at the larval to adult transition in C. elegans. Developmental cell *8*, 321-330.

Grosswendt, S., Filipchyk, A., Manzano, M., Klironomos, F., Schilling, M., Herzog, M., Gottwein, E., and Rajewsky, N. (2014). Unambiguous identification of miRNA:target site interactions by different types of ligation reactions. Molecular cell *54*, 1042-1054.

Hadley, W. (2016). Ggplot2 (New York, NY: Springer Science+Business Media, LLC).

He, Z., Zhang, H., Gao, S., Lercher, M.J., Chen, W.H., and Hu, S. (2016). Evolview v2: an online visualization and management tool for customized and annotated phylogenetic trees. Nucleic acids research *44*, W236-241.

Helwak, A., Kudla, G., Dudnakova, T., and Tollervey, D. (2013). Mapping the human miRNA interactome by CLASH reveals frequent noncanonical binding. Cell *153*, 654-665.

Hertel, J., Bartschat, S., Wintsche, A., Otto, C., Students of the Bioinformatics Computer, L., and Stadler, P.F. (2012). Evolution of the let-7 microRNA family. RNA biology *9*, 231-241.

Howe, K.L., Bolt, B.J., Cain, S., Chan, J., Chen, W.J., Davis, P., Done, J., Down, T., Gao, S., Grove, C.*, et al.* (2016). WormBase 2016: expanding to enable helminth genomic research. Nucleic acids research *44*, D774-780.

Howe, K.L., Bolt, B.J., Shafie, M., Kersey, P., and Berriman, M. (2017). WormBase ParaSite - a comprehensive resource for helminth genomics. Mol Biochem Parasitol *215*, 2-10.

Ilbay, O., and Ambros, V. (2019). Regulation of nuclear-cytoplasmic partitioning by the lin-28-lin-46 pathway reinforces microRNA repression of HBL-1 to confer robust cell-fate progression in C. elegans. Development *146*.

Ingolia, N.T. (2016). Ribosome Footprint Profiling of Translation throughout the Genome. Cell *165*, 22-33.

Ingolia, N.T., Brar, G.A., Rouskin, S., McGeachy, A.M., and Weissman, J.S. (2012). The ribosome profiling strategy for monitoring translation in vivo by deep sequencing of ribosome-protected mRNA fragments. Nature protocols *7*, 1534-1550.

John, B., Enright, A.J., Aravin, A., Tuschl, T., Sander, C., and Marks, D.S. (2004). Human MicroRNA targets. PLoS biology *2*, e363.

Kamath, R.S., Fraser, A.G., Dong, Y., Poulin, G., Durbin, R., Gotta, M., Kanapin, A., Le Bot, N., Moreno, S., Sohrmann, M.*, et al.* (2003). Systematic functional analysis of the Caenorhabditis elegans genome using RNAi. Nature *421*, 231-237.

Kozomara, A., Birgaoanu, M., and Griffiths-Jones, S. (2019). miRBase: from microRNA sequences to function. Nucleic acids research *47*, D155-D162.

Kucukural, A., Yukselen, O., Ozata, D.M., Moore, M.J., and Garber, M. (2019). DEBrowser: interactive differential expression analysis and visualization tool for count data. BMC genomics *20*, 6.

Lai, E.C. (2002). Micro RNAs are complementary to 3' UTR sequence motifs that mediate negative post-transcriptional regulation. Nature genetics *30*, 363-364.

Langmead, B., and Salzberg, S.L. (2012). Fast gapped-read alignment with Bowtie 2. Nature methods *9*, 357-359.

Lee, H., Han, S., Kwon, C.S., and Lee, D. (2016). Biogenesis and regulation of the let-7 miRNAs and their functional implications. Protein Cell *7*, 100-113.

Lee, R.C., Feinbaum, R.L., and Ambros, V. (1993). The C. elegans heterochronic gene lin-4 encodes small RNAs with antisense complementarity to lin-14. Cell *75*, 843-854.

Lewis, B.P., Burge, C.B., and Bartel, D.P. (2005). Conserved seed pairing, often flanked by adenosines, indicates that thousands of human genes are microRNA targets. Cell *120*, 15-20.

Liao, Y., Smyth, G.K., and Shi, W. (2014). featureCounts: an efficient general purpose program for assigning sequence reads to genomic features. Bioinformatics *30*, 923-930.

Lim, L.P., Lau, N.C., Garrett-Engele, P., Grimson, A., Schelter, J.M., Castle, J., Bartel, D.P., Linsley, P.S., and Johnson, J.M. (2005). Microarray analysis shows that some microRNAs downregulate large numbers of target mRNAs. Nature *433*, 769-773.

Lorenz, R., Bernhart, S.H., Honer Zu Siederdissen, C., Tafer, H., Flamm, C., Stadler, P.F., and Hofacker, I.L. (2011). ViennaRNA Package 2.0. Algorithms Mol Biol *6*, 26.

Love, M.I., Huber, W., and Anders, S. (2014). Moderated estimation of fold change and dispersion for RNA-seq data with DESeq2. Genome biology *15*, 550.

Martin, M. (2011). Cutadapt removes adapter sequences from high-throughput sequencing reads. 2011 *17*, 3.

Nelson, C., and Ambros, V. (2019). Trans-splicing of the C. elegans let-7 primary transcript developmentally regulates let-7 microRNA biogenesis and let-7 family microRNA activity. Development *146*.

Nelson, C., and Ambros, V. (2021). A cohort of Caenorhabditis species lacking the highly conserved let-7 microRNA. G3 Genes|Genomes|Genetics.

Nottrott, S., Simard, M.J., and Richter, J.D. (2006). Human let-7a miRNA blocks protein production on actively translating polyribosomes. Nature structural & molecular biology *13*, 1108-1114.

Pasquinelli, A.E., McCoy, A., Jimenez, E., Salo, E., Ruvkun, G., Martindale, M.Q., and Baguna, J. (2003). Expression of the 22 nucleotide let-7 heterochronic RNA throughout the Metazoa: a role in life history evolution? Evolution & development *5*, 372-378.

Paul, P., Chakraborty, A., Sarkar, D., Langthasa, M., Rahman, M., Bari, M., Singha, R.S., Malakar, A.K., and Chakraborty, S. (2018). Interplay between miRNAs and human diseases. Journal of cellular physiology *233*, 2007-2018.

Pawlica, P., Sheu-Gruttadauria, J., MacRae, I.J., and Steitz, J.A. (2020). How Complementary Targets Expose the microRNA 3' End for Tailing and Trimming during Target-Directed microRNA Degradation. Cold Spring Harbor symposia on quantitative biology.

Rehmsmeier, M., Steffen, P., Hochsmann, M., and Giegerich, R. (2004). Fast and effective prediction of microRNA/target duplexes. Rna *10*, 1507-1517.

Reinhart, B.J., Slack, F.J., Basson, M., Pasquinelli, A.E., Bettinger, J.C., Rougvie, A.E., Horvitz, H.R., and Ruvkun, G. (2000). The 21-nucleotide let-7 RNA regulates developmental timing in Caenorhabditis elegans. Nature *403*, 901-906.

Roush, S., and Slack, F.J. (2008). The let-7 family of microRNAs. Trends in cell biology *18*, 505-516.

Salomon, W.E., Jolly, S.M., Moore, M.J., Zamore, P.D., and Serebrov, V. (2015). Single-Molecule Imaging Reveals that Argonaute Reshapes the Binding Properties of Its Nucleic Acid Guides. Cell *162*, 84-95.

Santos, D.A., Shi, L., Tu, B.P., and Weissman, J.S. (2019). Cycloheximide can distort measurements of mRNA levels and translation efficiency. Nucleic acids research.

Schindelin, J., Arganda-Carreras, I., Frise, E., Kaynig, V., Longair, M., Pietzsch, T., Preibisch, S., Rueden, C., Saalfeld, S., Schmid, B.*, et al.* (2012). Fiji: an open-source platform for biological-image analysis. Nature methods *9*, 676-682.

Schirle, N.T., Sheu-Gruttadauria, J., and MacRae, I.J. (2014). Structural basis for microRNA targeting. Science *346*, 608-613.

Sheu-Gruttadauria, J., Pawlica, P., Klum, S.M., Wang, S., Yario, T.A., Schirle Oakdale, N.T., Steitz, J.A., and MacRae, I.J. (2019a). Structural Basis for Target-Directed MicroRNA Degradation. Molecular cell *75*, 1243-1255 e1247.

Sheu-Gruttadauria, J., Xiao, Y., Gebert, L.F., and MacRae, I.J. (2019b). Beyond the seed: structural basis for supplementary microRNA targeting by human Argonaute2. The EMBO journal.

Sokol, N.S., Xu, P., Jan, Y.N., and Ambros, V. (2008). Drosophila let-7 microRNA is required for remodeling of the neuromusculature during metamorphosis. Genes & development *22*, 1591-1596.

Spike, C.A., Coetzee, D., Eichten, C., Wang, X., Hansen, D., and Greenstein, D. (2014). The TRIM-NHL protein LIN-41 and the OMA RNA-binding proteins antagonistically control the prophase-to-metaphase transition and growth of Caenorhabditis elegans oocytes. Genetics *198*, 1535-1558.

Sulston, J.E., Schierenberg, E., White, J.G., and Thomson, J.N. (1983). The embryonic cell lineage of the nematode Caenorhabditis elegans. Developmental biology *100*, 64-119.

Tennessen, J.M., and Thummel, C.S. (2008). Developmental timing: let-7 function conserved through evolution. Current biology : CB *18*, R707-708.

Timmons, L., Court, D.L., and Fire, A. (2001). Ingestion of bacterially expressed dsRNAs can produce specific and potent genetic interference in Caenorhabditis elegans. Gene *263*, 103-112.

Veksler-Lublinsky, I., Shemer-Avni, Y., Kedem, K., and Ziv-Ukelson, M. (2010). Gene bi-targeting by viral and human miRNAs. BMC bioinformatics *11*, 249.

Vella, M.C., Choi, E.Y., Lin, S.Y., Reinert, K., and Slack, F.J. (2004). The C. elegans microRNA let-7 binds to imperfect let-7 complementary sites from the lin-41 3'UTR. Genes & development *18*, 132-137.

Wahlquist, C., Jeong, D., Rojas-Munoz, A., Kho, C., Lee, A., Mitsuyama, S., van Mil, A., Park, W.J., Sluijter, J.P., Doevendans, P.A.*, et al.* (2014). Inhibition of miR-25 improves cardiac contractility in the failing heart. Nature *508*, 531-535.

Wee, L.M., Flores-Jasso, C.F., Salomon, W.E., and Zamore, P.D. (2012). Argonaute divides its RNA guide into domains with distinct functions and RNA-binding properties. Cell *151*, 1055-1067.

Wolter, J.M., Le, H.H., Linse, A., Godlove, V.A., Nguyen, T.D., Kotagama, K., Lynch, A., Rawls, A., and Mangone, M. (2017). Evolutionary patterns of metazoan microRNAs reveal targeting principles in the let-7 and miR-10 families. Genome research *27*, 53-63.

Worringer, K.A., Rand, T.A., Hayashi, Y., Sami, S., Takahashi, K., Tanabe, K., Narita, M., Srivastava, D., and Yamanaka, S. (2014). The let-7/LIN-41 pathway regulates reprogramming to human induced pluripotent stem cells by controlling expression of prodifferentiation genes. Cell stem cell *14*, 40-52.

Wu, L., Fan, J., and Belasco, J.G. (2006). MicroRNAs direct rapid deadenylation of mRNA. Proceedings of the National Academy of Sciences of the United States of America *103*, 4034-4039.

Xiao, Y., and MacRae, I.J. (2020). Robust differential microRNA targeting driven by supplementary interactions in vitro. Rna *26*, 162-174.

Zhang, Z., Theurkauf, W.E., Weng, Z., and Zamore, P.D. (2012). Strand-specific libraries for high throughput RNA sequencing (RNA-Seq) prepared without poly(A) selection. Silence *3*, 9.

927

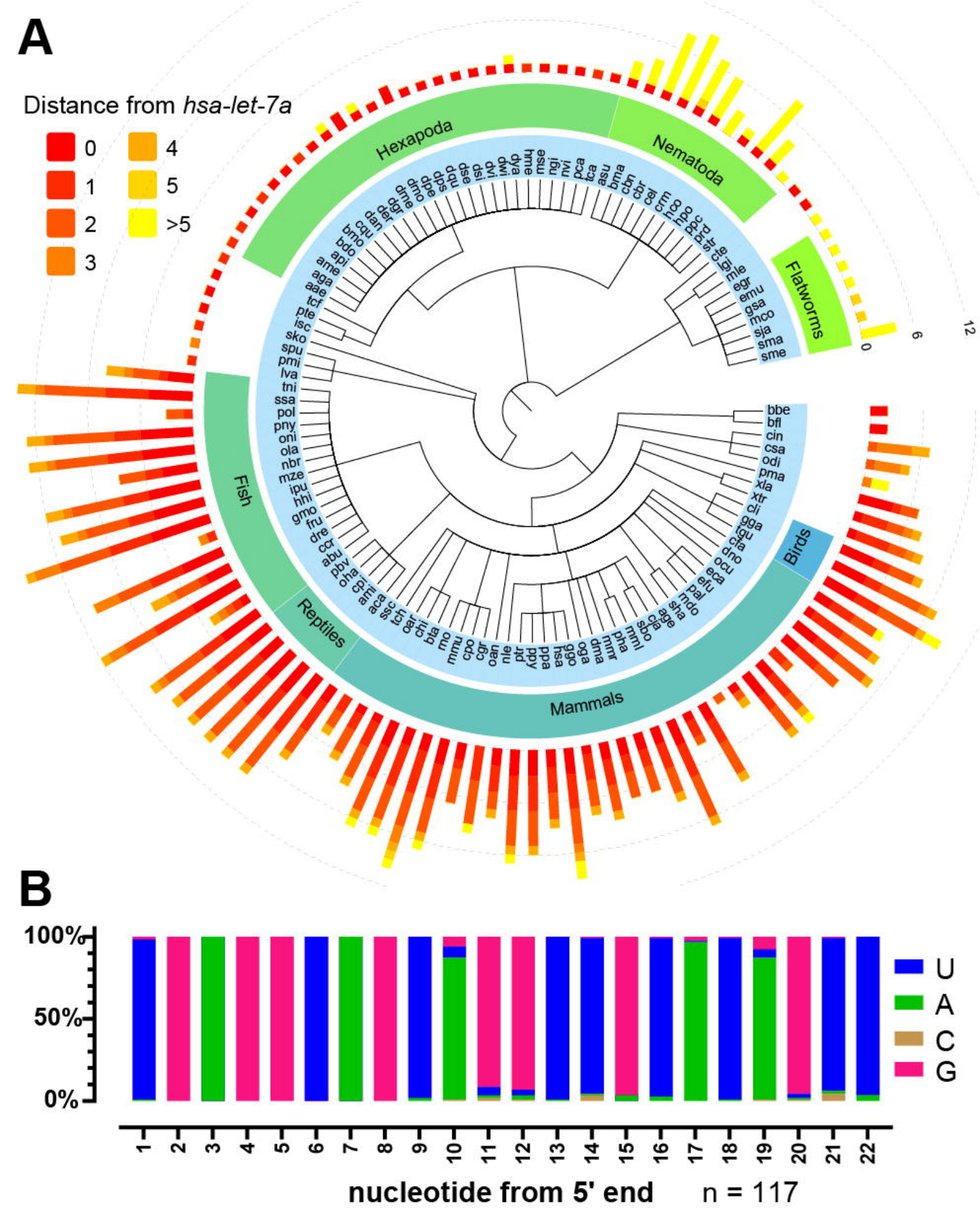
A
Distance from hsa-let-7a
0
1
2
3
4
5
>5
Hexapoda
Nematoda
Flatworms
Fish
Reptiles
Birds
Mammals
0
6
12
B
100%
50%
0%
U
A
C
G
1 2 3 4 5 6 7 8 9 10 11 12 13 14 15 16 17 18 19 20 21 22
nucleotide from 5' end
n = 117

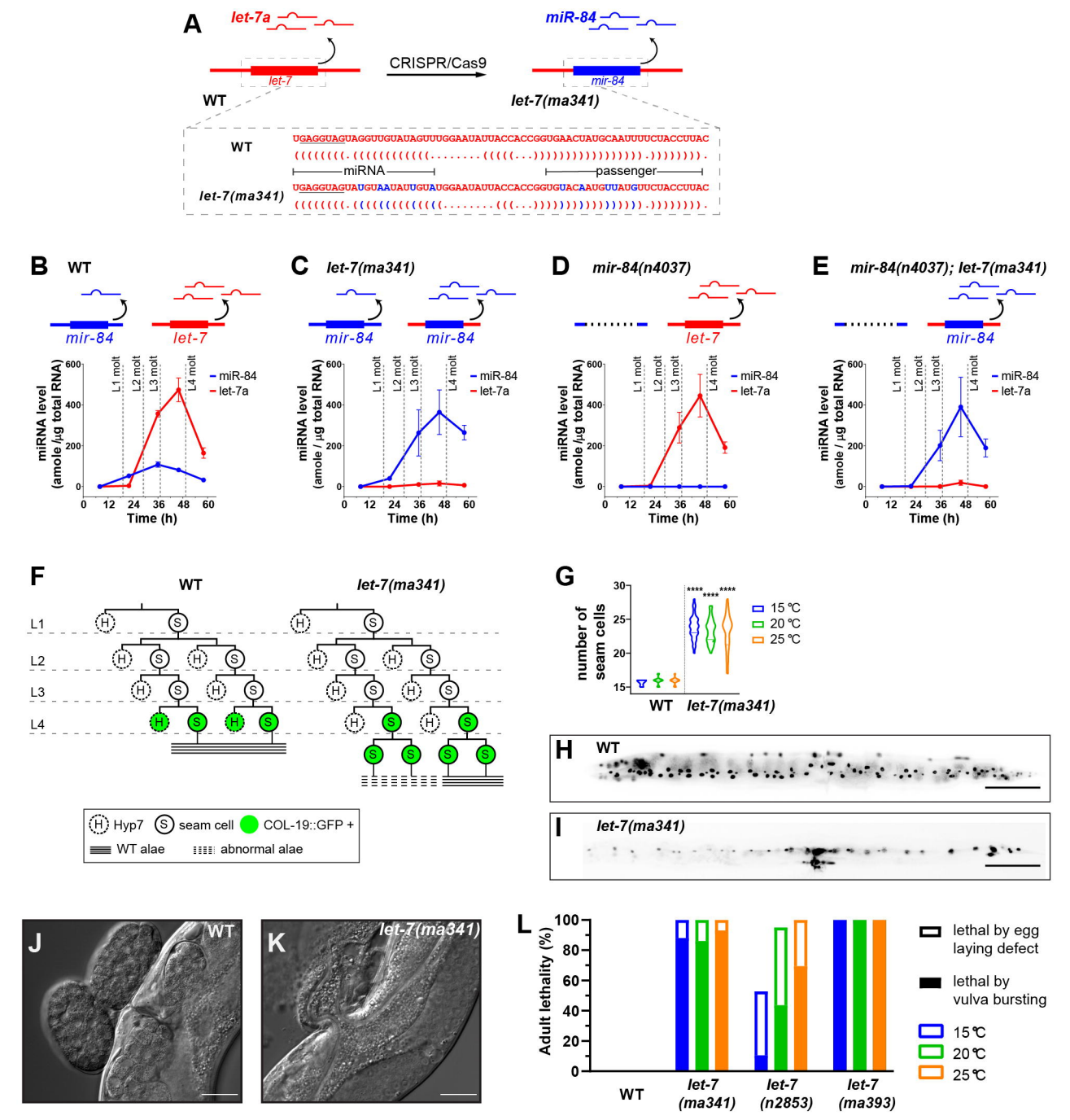
A
let-7a
let-7
WT
CRISPR/Cas9
miR-84
mir-84
let-7(ma341)
WT
UGAGGUAGUAGGUUGUAUAGUUUGGAAUAUUACCACCGGUGAACUAUGCAAUUUUCUACCUUAC
miRNA
passenger
let-7(ma341)
UGAGGUAGUAUGUAAUAUUGUAUGGAAUAUUACCACCGGUGUACAAUGUUAUGUUCUACCUUAC
B WT
mir-84
let-7
C let-7(ma341)
mir-84
mir-84
D mir-84(n4037)
let-7
E mir-84(n4037); let-7(ma341)
mir-84
miR-84
let-7a
L1 molt
L2 molt
L3 molt
L4 molt
miRNA level (amole /µg total RNA)
Time (h)
F
WT
let-7(ma341)
L1
L2
L3
L4
Hyp7
seam cell
COL-19::GFP +
WT alae
abnormal alae
G
number of seam cells
15 ℃
20 ℃
25 ℃
WT
let-7(ma341)
H WT
I let-7(ma341)
J WT
K let-7(ma341)
L
Adult lethality (%)
WT
let-7 (ma341)
let-7 (n2853)
let-7 (ma393)
lethal by egg laying defect
lethal by vulva bursting
15 ℃
20 ℃
25 ℃

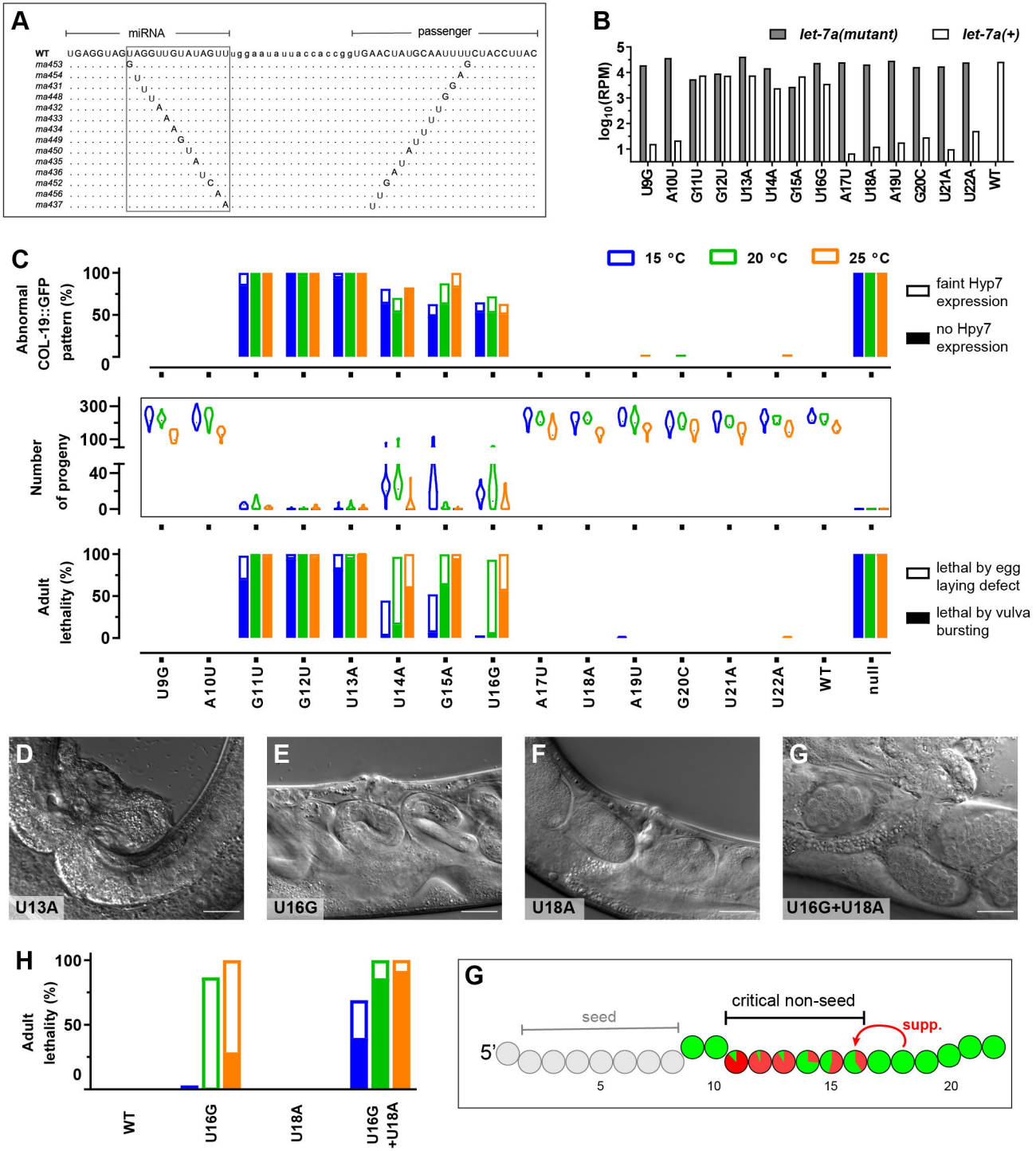
A
miRNA
passenger
WT UGAGGUAGUAGGUUGUAUAGUUuggaauauuaccaccggUGAACUAUGCAAUUUUCUACCUUAC
ma453
ma454
ma431
ma448
ma432
ma433
ma434
ma449
ma450
ma435
ma436
ma452
ma456
ma437
B
let-7a(mutant)
let-7a(+)
log10(RPM)
U9G
A10U
G11U
G12U
U13A
U14A
G15A
U16G
A17U
U18A
A19U
G20C
U21A
U22A
WT
C
15 °C
20 °C
25 °C
Abnormal COL-19::GFP pattern (%)
faint Hyp7 expression
no Hpy7 expression
Number of progeny
Adult lethality (%)
lethal by egg laying defect
lethal by vulva bursting
null
D
U13A
E
U16G
F
U18A
G
U16G+U18A
H
Adult lethality (%)
WT
U16G
U18A
U16G +U18A
G
seed
critical non-seed
supp.
5'
5
10
15
20

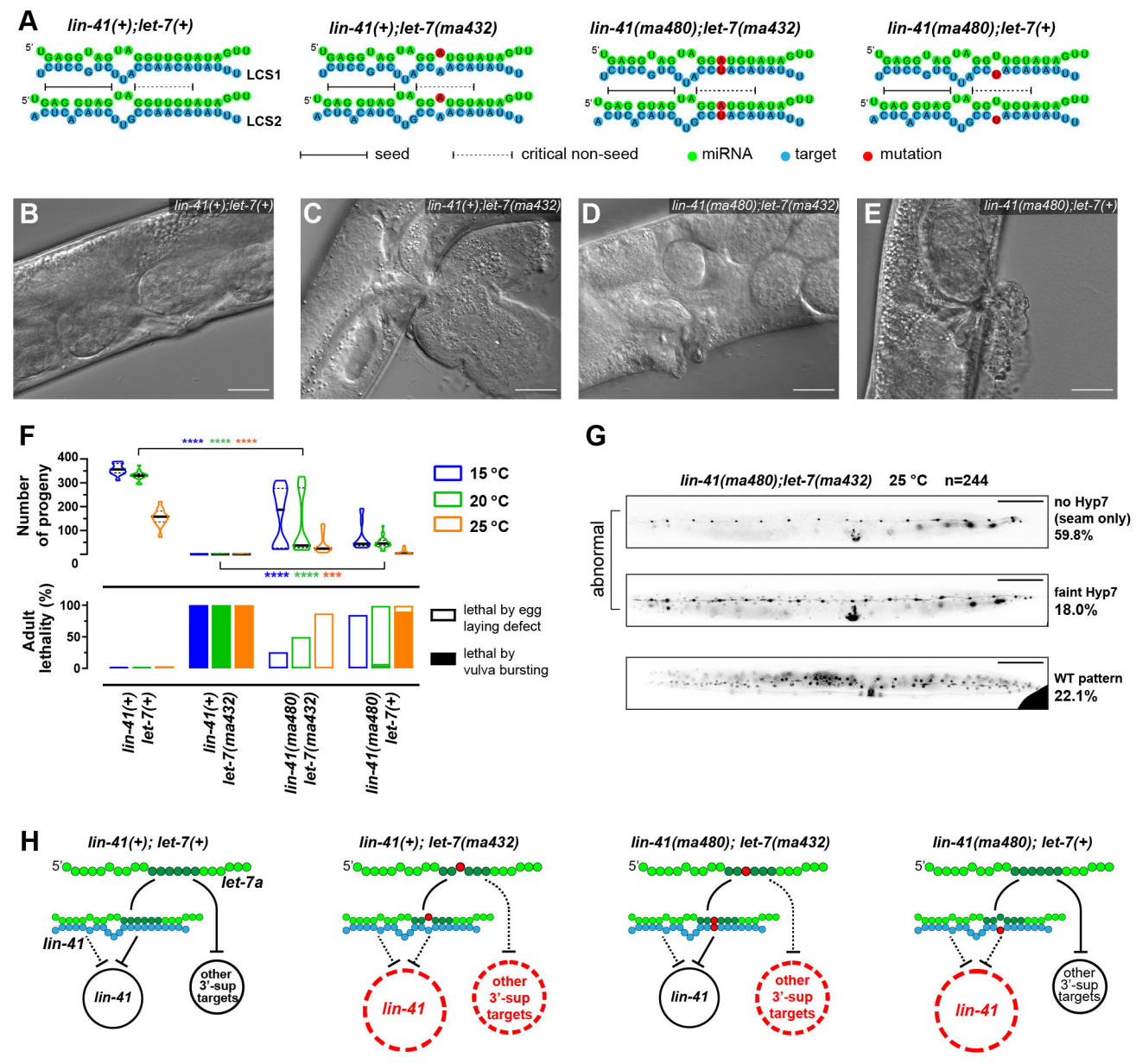
A
lin-41(+);let-7(+)
lin-41(+);let-7(ma432)
lin-41(ma480);let-7(ma432)
lin-41(ma480);let-7(+)
LCS1
LCS2
seed
critical non-seed
miRNA
target
mutation
B
lin-41(+);let-7(+)
C
lin-41(+);let-7(ma432)
D
lin-41(ma480);let-7(ma432)
E
lin-41(ma480);let-7(+)
F
Number of progeny
Adult lethality (%)
15 °C
20 °C
25 °C
lethal by egg laying defect
lethal by vulva bursting
lin-41(+) let-7(+)
lin-41(+) let-7(ma432)
lin-41(ma480) let-7(ma432)
lin-41(ma480) let-7(+)
G
lin-41(ma480);let-7(ma432) 25 °C n=244
abnormal
no Hyp7 (seam only) 59.8%
faint Hyp7 18.0%
WT pattern 22.1%
H
lin-41(+); let-7(+)
lin-41(+); let-7(ma432)
lin-41(ma480); let-7(ma432)
lin-41(ma480); let-7(+)
let-7a
lin-41
other 3'-sup targets

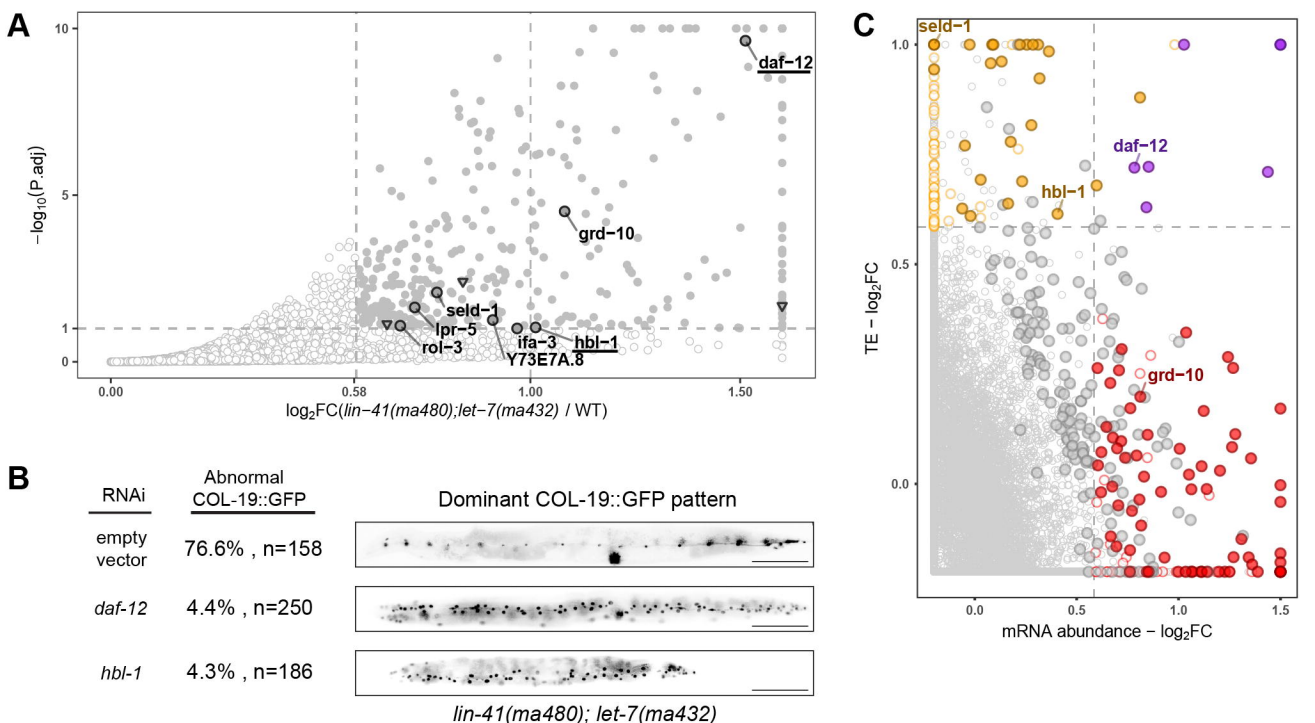
A
daf−12
grd−10
seld−1
lpr−5
rol−3
ifa−3
hbl−1
Y73E7A.8
−log10(P.adj)
log2FC(lin−41(ma480);let−7(ma432) / WT)
B
RNAi
Abnormal COL-19::GFP
Dominant COL-19::GFP pattern
empty vector
76.6% , n=158
daf-12
4.4% , n=250
hbl-1
4.3% , n=186
lin-41(ma480); let-7(ma432)
C
seld−1
daf−12
hbl−1
grd−10
TE − log2FC
mRNA abundance − log2FC

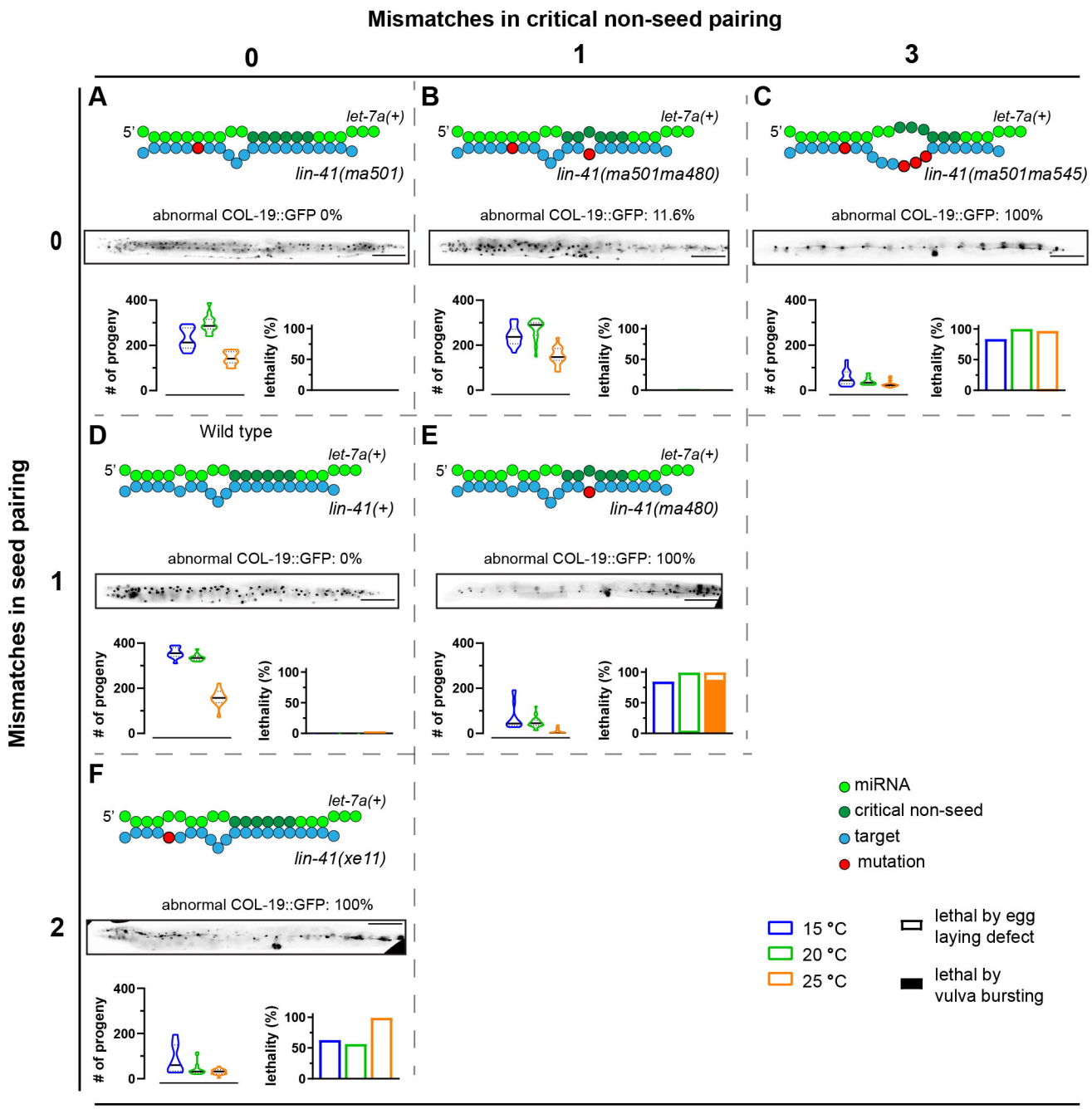
Mismatches in critical non-seed pairing
0
1
3
Mismatches in seed pairing
0
1
2
A
let-7a(+)
5'
lin-41(ma501)
abnormal COL-19::GFP 0%
B
let-7a(+)
5'
lin-41(ma501ma480)
abnormal COL-19::GFP: 11.6%
C
let-7a(+)
5'
lin-41(ma501ma545)
abnormal COL-19::GFP: 100%
D
Wild type
let-7a(+)
5'
lin-41(+)
abnormal COL-19::GFP: 0%
E
let-7a(+)
5'
lin-41(ma480)
abnormal COL-19::GFP: 100%
F
let-7a(+)
5'
lin-41(xe11)
abnormal COL-19::GFP: 100%
# of progeny
lethality (%)
miRNA
critical non-seed
target
mutation
15 °C
20 °C
25 °C
lethal by egg laying defect
lethal by vulva bursting

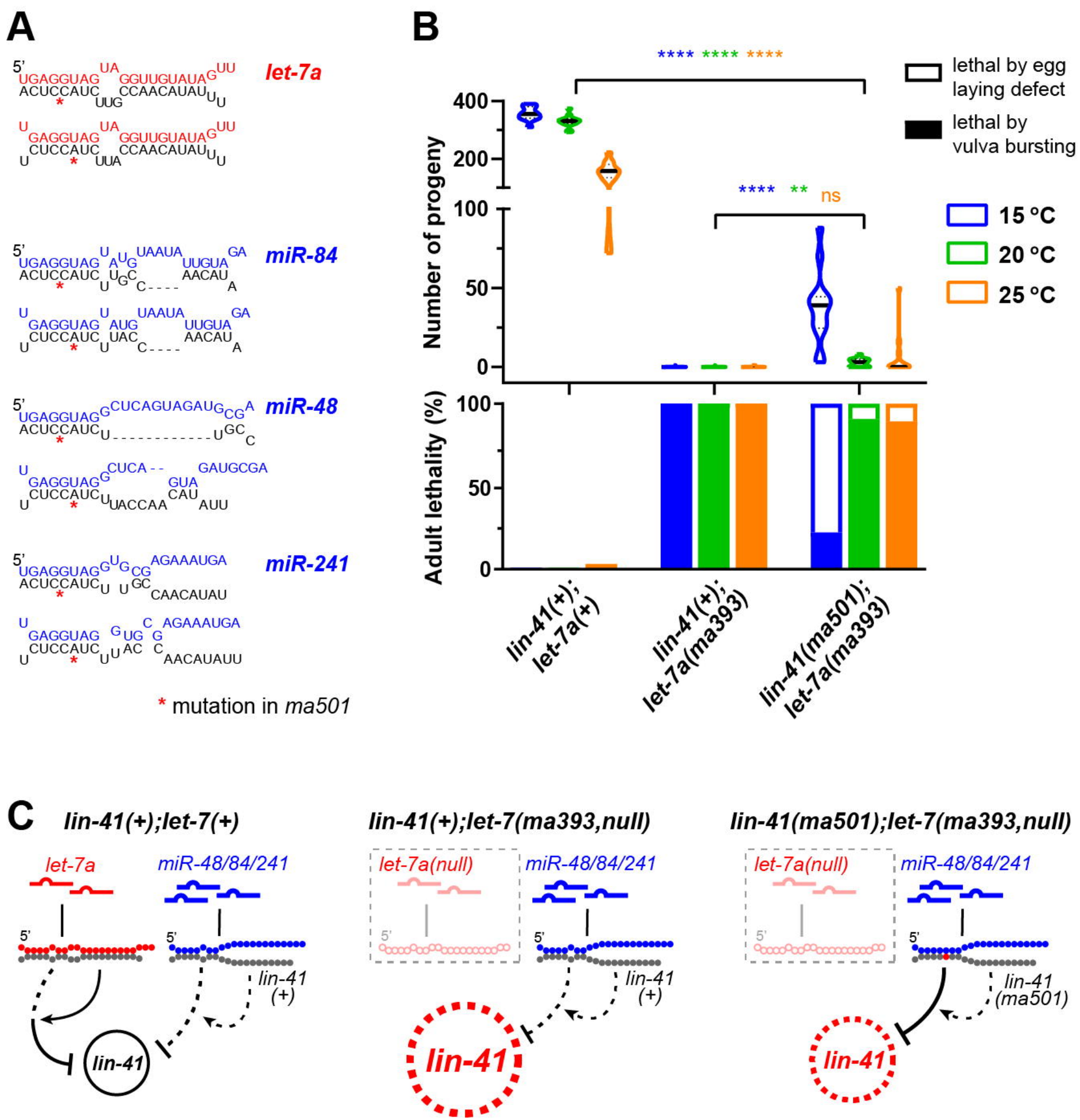
A
let-7a
miR-84
miR-48
miR-241
* mutation in ma501
B
lethal by egg laying defect
lethal by vulva bursting
15 °C
20 °C
25 °C
Number of progeny
Adult lethality (%)
lin-41(+); let-7a(+)
lin-41(+); let-7a(ma393)
lin-41(ma501); let-7a(ma393)
C
lin-41(+);let-7(+)
lin-41(+);let-7(ma393,null)
lin-41(ma501);let-7(ma393,null)
let-7a
miR-48/84/241
let-7a(null)
lin-41 (+)
lin-41 (ma501)
lin-41